

Supporting Information

Hydrogen Spillover Drives Room Temperature Sensing on Spark Plasma Sintered BaTiO₃ with Pt Electrodes

Jon G. Bell¹, Shangxiong Huangfu¹, Luca Artiglia², Thomas Graule¹, and Michael Stuer¹

¹ High Performance Ceramics Laboratory, Department of Advanced Materials and Surfaces, Swiss Federal Laboratories for Materials Science and Technology, Dübendorf, Switzerland.

² Swiss Light Source, Paul Scherrer Institute, Villigen, Switzerland.

Contents

1	Experimental	3
1.1	Material Synthesis and Characterisation	3
1.1.1	Powder Properties: Gas Adsorption and Surface Area	3
1.1.2	Powder Properties: Laser Diffraction for Particle Size Measurements	4
1.2	Spark Plasma Sintering of BaTiO ₃	5
1.3	Scanning Electron Microscopy (SEM)	7
1.4	Powder X-ray diffraction (PXRD)	7
1.5	Post-Synthetic Reduction and Oxidation Program to Incorporate Ionsorbed Oxygen Species	8
1.6	Total Resistance Increase During Oxidation	9
1.7	Electrochemical Impedance Spectroscopy (EIS)	9
1.7.1	Kramers Kronig Analysis	9
2	Results and Discussion	11
2.1	Scanning Electron Microscopy	11
2.2	Sintered Pellet Density and N ₂ Surface Area Measurements	11
2.3	Powder X-Ray Diffraction (PXRD)	12
2.4	Controlled Oxidation	13
2.4.1	Oxidation at 460 °C	13
2.4.2	Oxidation at 470 °C	14
2.5	Gas Sensing: Switching from Air to H ₂ to Air at 22 °C	14
2.5.1	Sample oxidised at 460 °C	14
2.6	Electrochemical Impedance Spectroscopy Response in N ₂ and O ₂	15
2.7	Near Ambient Pressure X-Ray Photoelectron Spectroscopy (NAP-XPS)	17
2.7.1	Quality Assessment of XPS Peak Fitting	18
2.7.2	O 1s Photoemission Peak for Pt-BTO-470	19
2.7.3	C 1s Photoemission Peak for Pt-BTO-470	22

2.7.4	Ti 2p Photoemission Peak for Pt-BTO-470.....	24
2.7.5	Ba 4d Photoemission Peak for Pt-BTO-470	26
2.7.6	Pt 4f Photoemission Peak for Pt-BTO-470	28
2.8	Electrochemical Impedance Spectroscopy Studies.....	30
2.8.1	H_2 and D_2 Kinetic isotope Studies at 22 °C and 130 °C.....	30
2.8.2	AC Conductivity Analysis: Jonscher Analysis as a Function of H_2 Concentration and Temperature	31
2.8.3	Langmuir Conductivity Model.....	39
2.8.4	Charge Transport Mechanism from Jonscher Model S Parameter (S vs. T)	40
2.8.5	Capacitance Measurements and Colossal Relative Permittivity (ϵ_r)	43
2.8.6	Distribution of Relaxation Times Analysis (DRT)	45
2.8.7	Activation Energies from Jonscher Analysis using σ_{dc} Data.....	61
2.8.8	Meyer-Neldel Effect for Total Conductivity from Jonscher σ_{dc} Data	64
2.8.9	Grain Boundary Activation Energies from DRT Analysis	65
2.8.10	Meyer-Neldel Effect for Grain Boundary Regions from Distribution of Relaxation Times Analysis.....	65
3	References	67

1 Experimental

1.1 Material Synthesis and Characterisation

1.1.1 Powder Properties: Gas Adsorption and Surface Area

The N₂ surface areas of BaTiO₃ powders and sintered pellets were measured at -196 °C using a Micromeritics 2020 ASAP volumetric adsorption system. Approximately 2 grams of each sample type was placed into the sample tube and a displacer rod was added. The sample chamber was heated to 150 °C and evacuated to a pressure of 13 µbar over a 1-hour period. Following this, the samples were kept at 150 °C and degassed for 2 hours. After degassing, samples were cooled to room temperature and weighed to attain the dry weight. The sample tubes were attached to the instrument measuring ports, and isothermal measurements were performed using a Dewar filled with liquid nitrogen for adsorption at -196 °C. N₂ adsorption was performed on the degassed materials at -196 °C using a high-resolution isotherm up to a N₂ relative pressure (p/p⁰) equal to 0.98. Surface areas were calculated using the Brunauer-Emmett-Teller (BET) multilayer adsorption equation.

Table S 1. BaTiO₃ powder properties: Density, N₂ BET surface area and diameter, and laser diffraction D_{v50} value.

Sample	He pycnometry density (g cm ⁻³)	N ₂ BET surface area (m ² g ⁻¹)	BET diameter (µm)	D _{v50} (µm)	Aggregation factor
BaTiO ₃ powder	5.72	1.93 ± 0.15	0.54 ± 0.04	0.60 ± 0.14	1.1

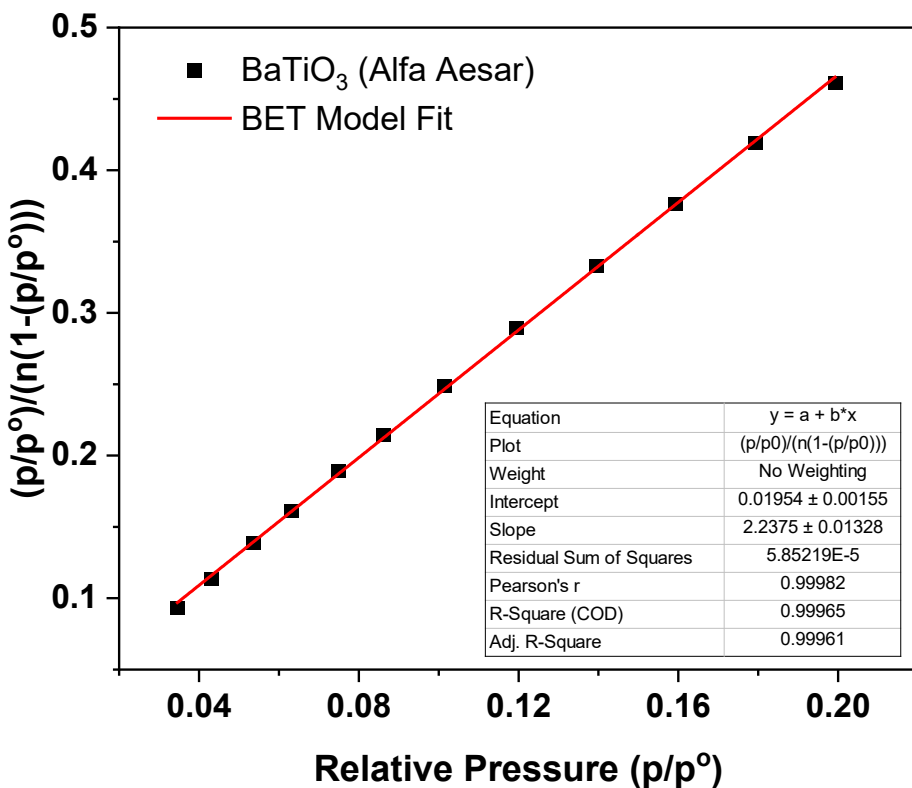


Figure S 1. BET plot for N₂ adsorption on BaTiO₃ as-received powder at -196 °C.

1.1.2 Powder Properties: Laser Diffraction for Particle Size Measurements

BaTiO₃ (0.4 grams) was mixed with 40 mL of ultrapure water. The suspension was sonicated for 15 minutes with an ultrasound tip. The particle size measurement was performed with a Beckman Coulter LS 13 320 laser diffraction particle size analyser. Particle size (μm) vs. the differential volume is shown in SI Figure 2.

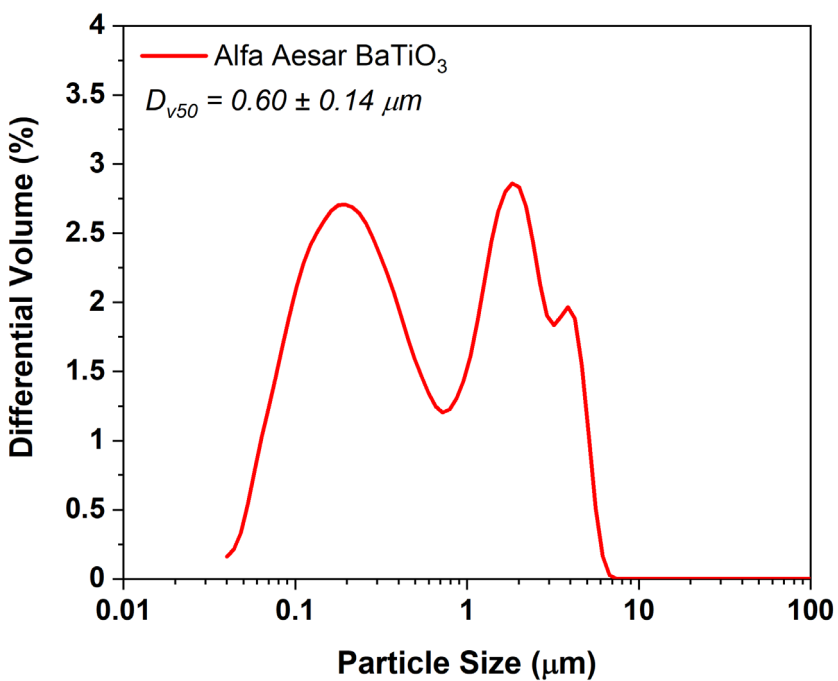


Figure S 2. Particle size laser diffraction measurement of as-received BaTiO₃ powder.

1.2 Spark Plasma Sintering of BaTiO₃

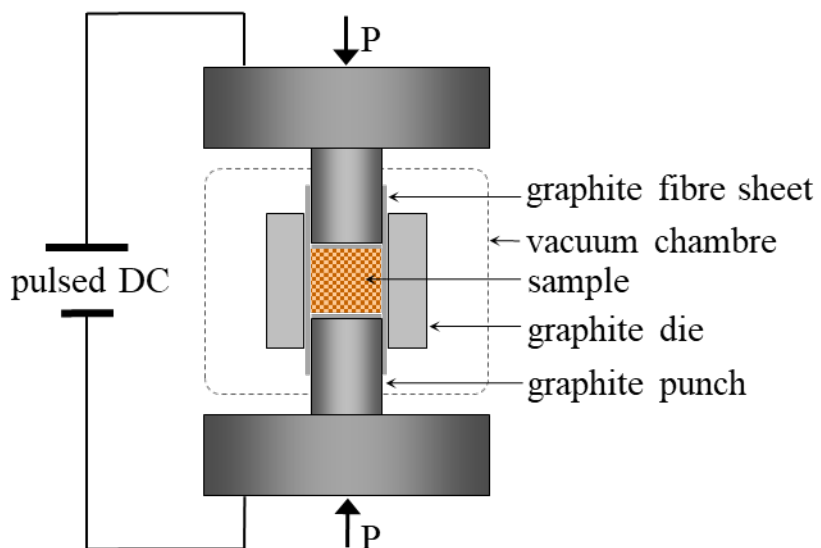
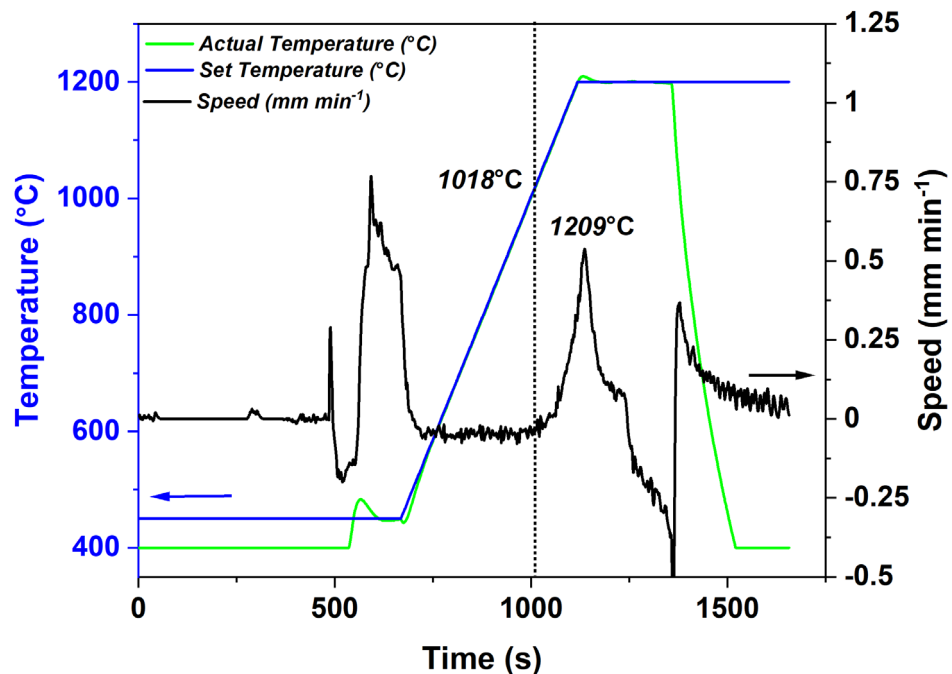


Figure S 3. Schematic diagram of the spark plasma sintering setup used in this study. Conditions used: heating rate – 100 °C min⁻¹; sintering temperature – 1200 °C; Pressure - 50 MPa; pulse sequence 12:6.

(a)



(b)

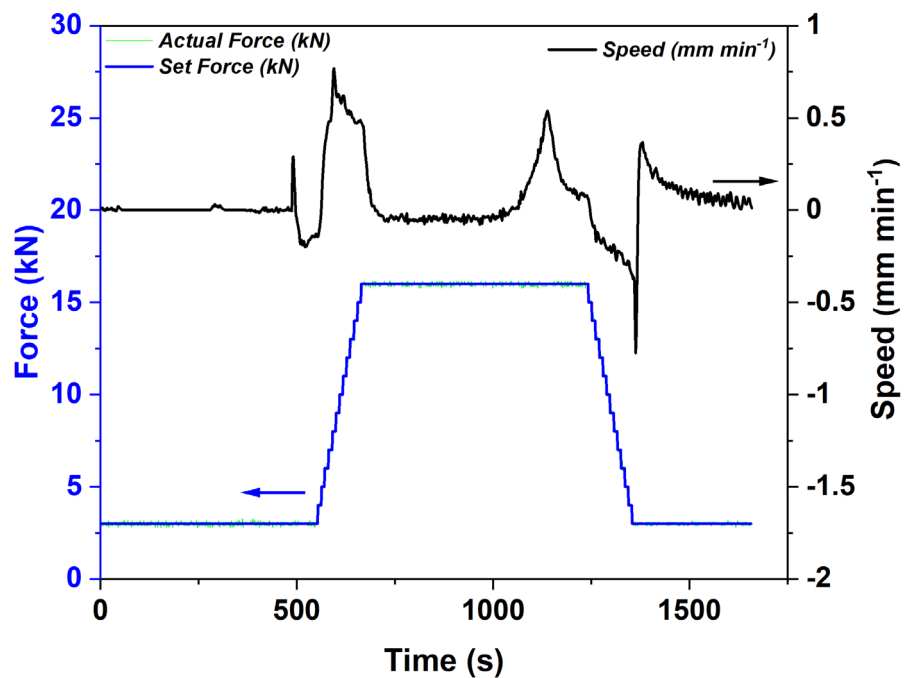


Figure S 4. Spark plasma sintering programs for BTO sintered at 1200 °C and pressed at 16 kN (50 MPa for 20 mm diameter sample) showing (a) temperature and speed vs. time and (b) force and speed vs. time.

1.3 Scanning Electron Microscopy (SEM)

Scanning electron micrographs were collected using a FEI Helios NanoLab 660 dual beam scanning electron microscope to determine the microstructure of the spark plasma sintered BaTiO₃ polished pellets. The sample was mounted on an SEM stub using carbon double sided adhesive tape.

1.4 Powder X-ray diffraction (PXRD)

PXRD profiles were measured on a PANalytical X'Pert Pro MPD, powered by a Philips PW3040/60 X-ray generator using Cu Ka radiation ($\lambda = 1.540598$ Angstroms) at 40 kV and a current of 40 mA. X-ray diffraction patterns were measured using a PW3050/60 goniometer and a PW3064/60 reflection-transmission sample stage with a revolution time of 8 seconds. The incident beam optics comprised a Nickle beta filter, 0.04 radian Soller slits, a 15mm fixed incident beam mask, a 1/4° divergence slit, and a 1/2° anti-scatter slit. The diffracted beam optics were composed of 0.04 radian Soller slits, a 5.0 mm anti-scatter slit, and a PIXcel1D-Medipix3 detector in scanning line detector (1D) mode. The total scan time was 8.5 hours, and the final spectra consisted of a superposition of two runs. The program for each run employed a 5°–140° 2θ scanning range with a 90 ms dwell time and a scan step size of 0.0033°. XRD diffraction spectra were fit to the identified phases using the HighScore Plus software. Following background subtraction and spectra peak determination, phases were identified and matched from the Crystallographic Open Database (COD).

1.5 Post-Synthetic Reduction and Oxidation Program to Incorporate Ionosorbed Oxygen Species

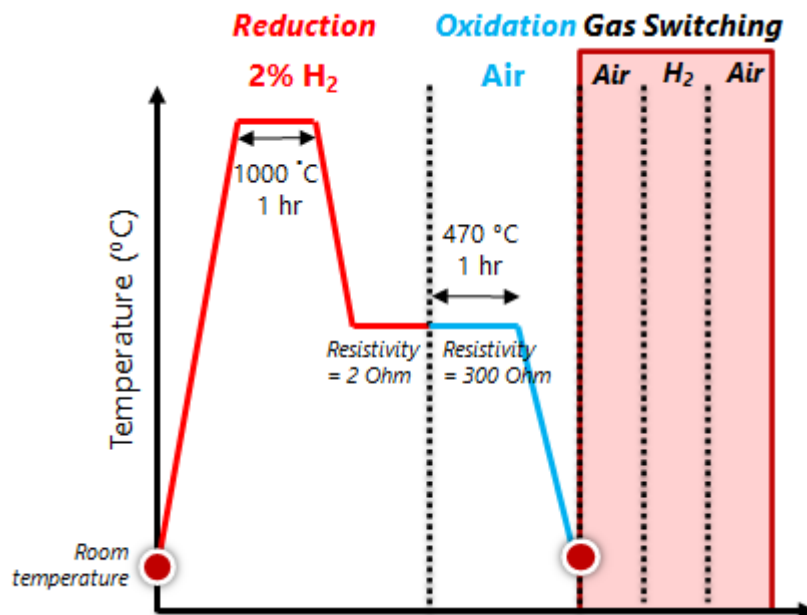


Figure S 5. Diagrammatic representation of the temperature and gas treatment program used to generate H₂ sensing Pt-BTO, involving reduction in 2% H₂ at 1000 °C for 1 hour, followed by partial reoxidation at 460 °C and 470 °C for 75 and 55 minutes, respectively. The initial gas switching experiments were performed at room temperature and by switching from flowing air (250 ml min⁻¹) to 2% H₂ in Ar and then back to air.

1.6 Total Resistance Increase During Oxidation

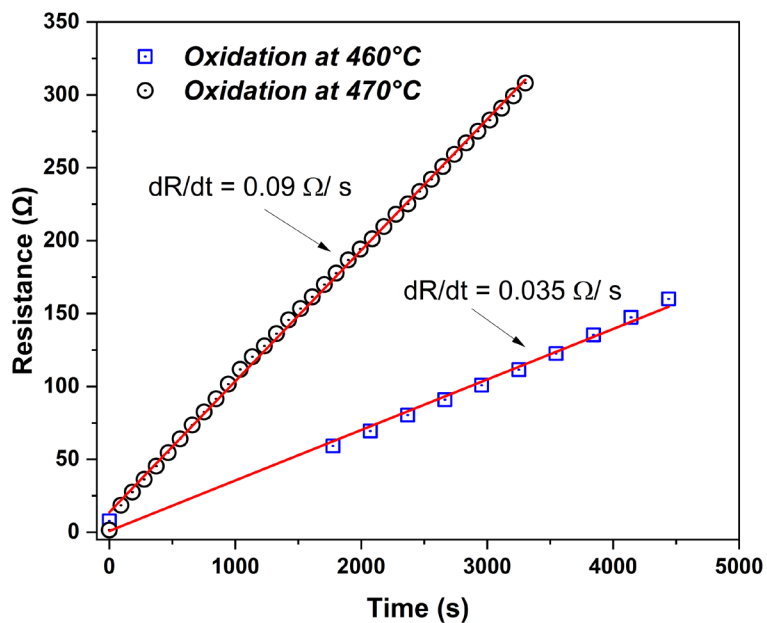
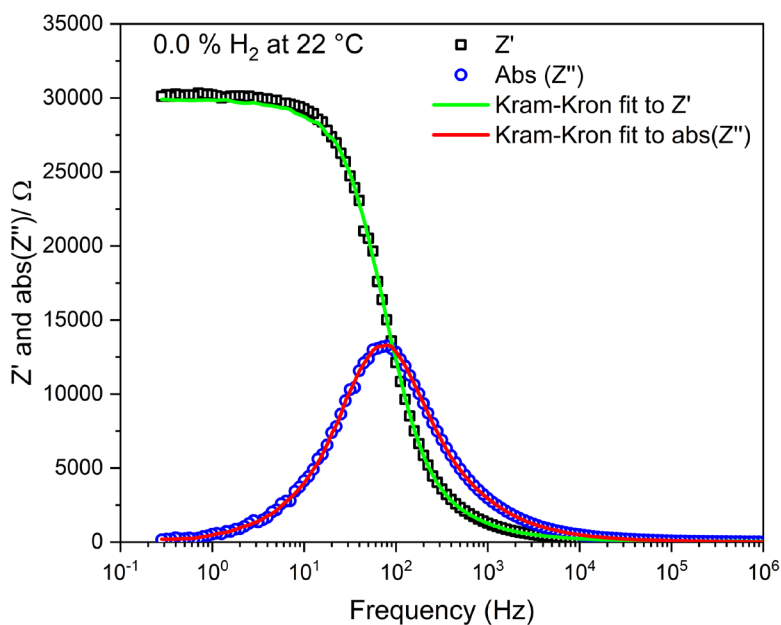


Figure S 6. Increase in the resistance of Pt-BTO during reoxidation under air (250 ml min^{-1}) at 460°C and 470°C .

1.7 Electrochemical Impedance Spectroscopy (EIS)

1.7.1 Kramers Kronig Analysis

a)



b)

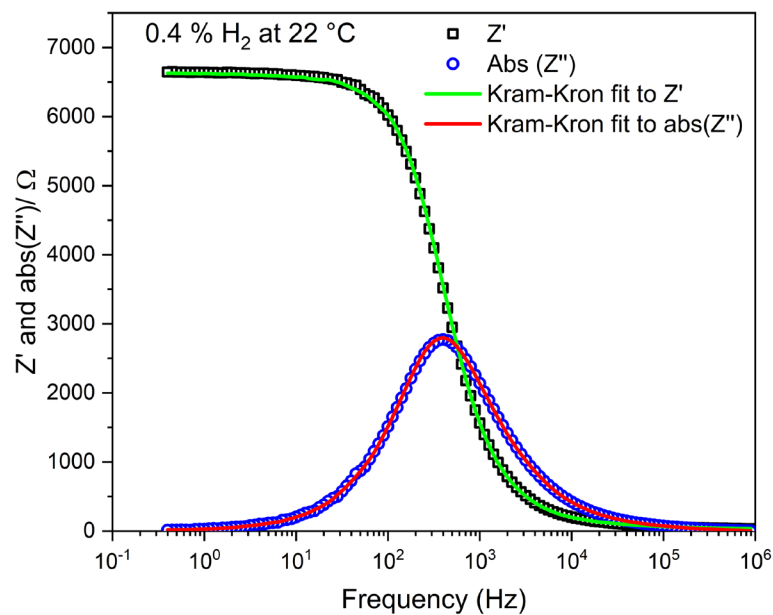


Figure S 7. Kramers-Kronig model fitting to high resolution impedance data (30 points per decade) for Pt-BTO-470 at 22 °C and exposed to 0.4% H₂ in N₂ showing that the measurement system obeys the rules of linearity, time invariance, and causality.

2 Results and Discussion

2.1 Scanning Electron Microscopy

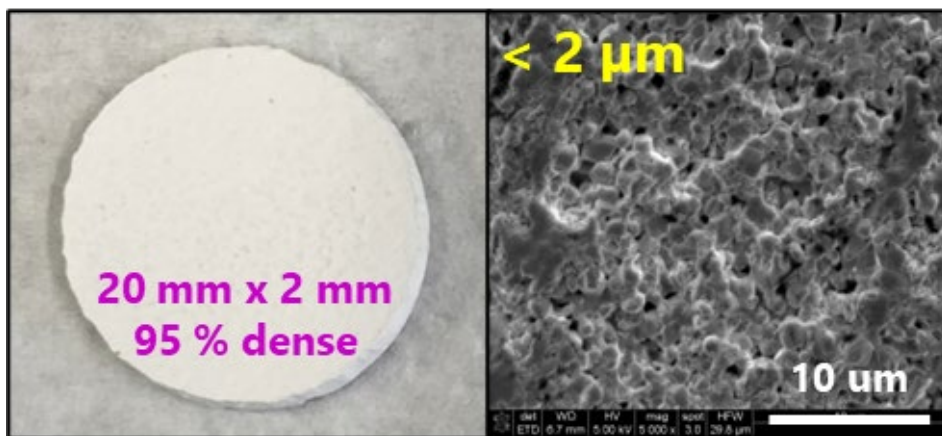


Figure S 8. (Left) BaTiO₃ pellet after spark plasma sintering in argon at 1200 °C and pressing at 50 MPa, designated was BTO-SPS. (Right) scanning electron micrograph of BTO pellet showing granular morphology.

2.2 Sintered Pellet Density and N₂ Surface Area Measurements

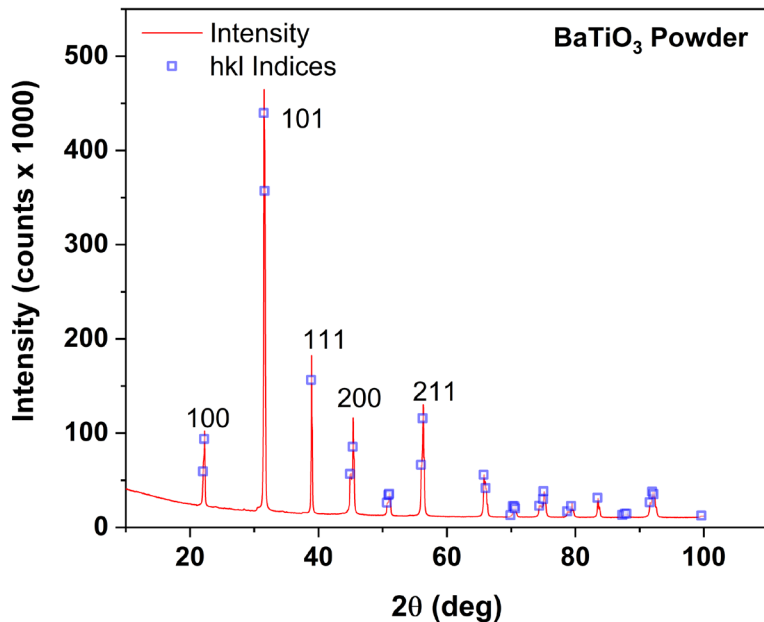
Density measurements were performed using the Archimedes method on a Mettler Toledo XP-205DR balance with a density measurement accessory. Samples were dried at 120 °C for 12 hours prior to density measurements. Ultra-pure water was degassed under vacuum and magnetically stirred for 3 hours prior to the density measurements.

Table S 2. SPS BTO pellet properties: density and porosity characterisation for samples.

Sample	Arch. Density (g cm ⁻³)	Relative Density (%)	N ₂ BET Surface Area (m ² /g)
SPS BTO pellet	5.736	95.3	0.20 ± 0.04

2.3 Powder X-Ray Diffraction (PXRD)

a)



b)

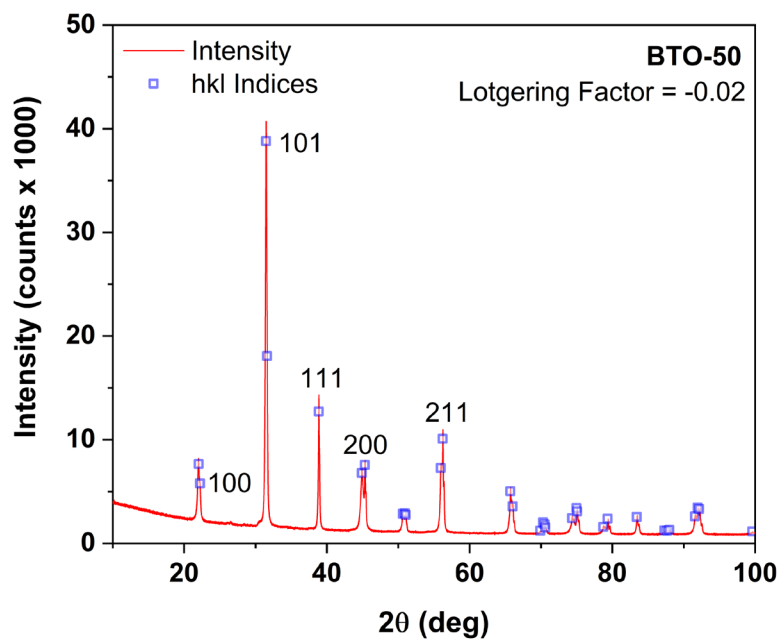
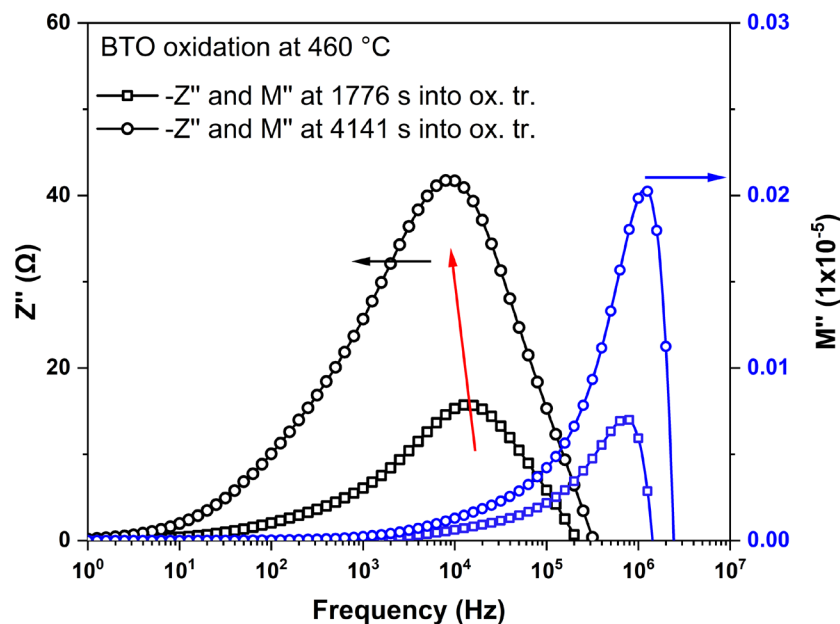


Figure S 9. Powder x-ray diffraction spectra of (a) as-received BaTiO₃ powder and (b) BTO spark plasma sintered sample, showing phase-pure and textureless BaTiO₃ (as calculated by the Lotgering factor).

2.4 Controlled Oxidation

2.4.1 Oxidation at 460 °C

a)



b)

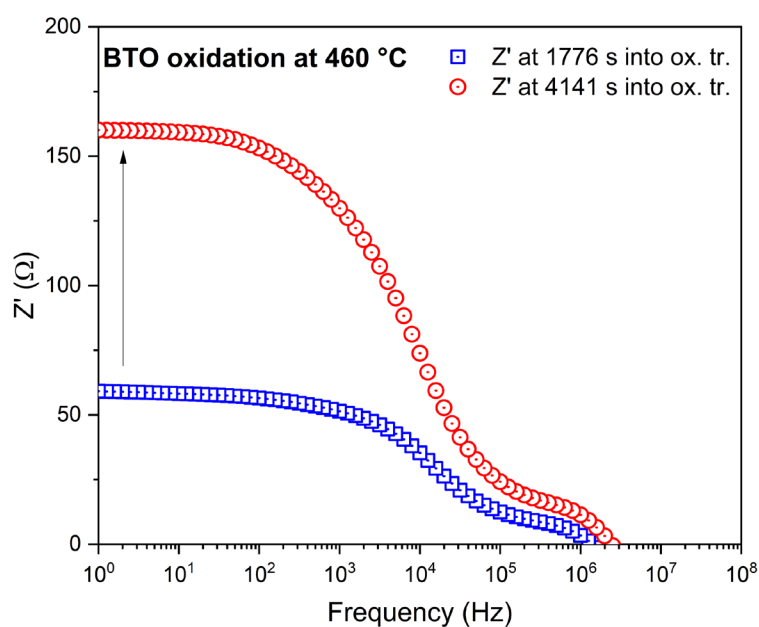


Figure S 10. Spectroscopic plots of (a) Z'' and M'' vs. frequency and (b) Z' vs. frequency for Pt-BTO during oxidation at 460 °C under flowing air (250 ml min^{-1}), forming Pt-BTO-460.

2.4.2 Oxidation at 470 °C

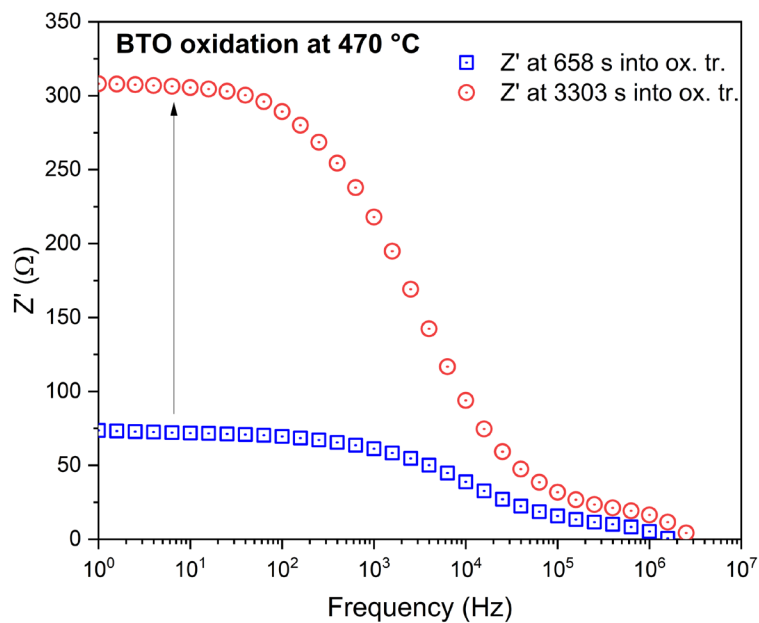
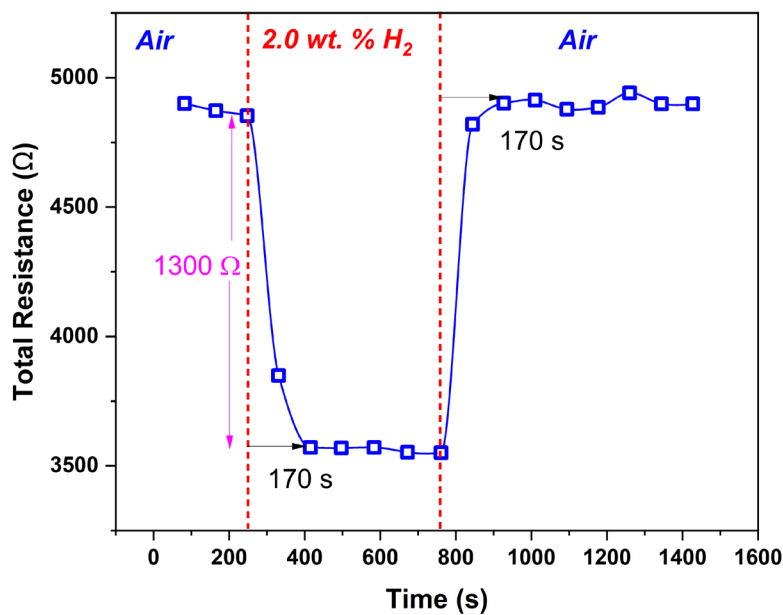


Figure S 11. Spectroscopic plots of (a) Z'' and M'' vs. frequency and (b) Z' vs. frequency for Pt-BTO during oxidation at 470 °C under flowing air (250 ml min^{-1}), forming Pt-BTO-470.

2.5 Gas Sensing: Switching from Air to H₂ to Air at 22 °C

2.5.1 Sample oxidised at 460 °C

a)



b)

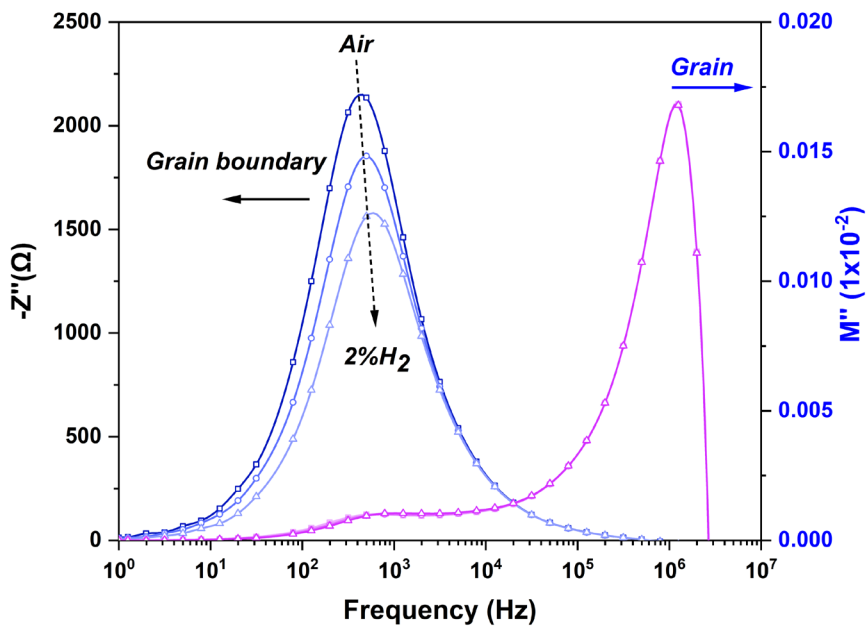
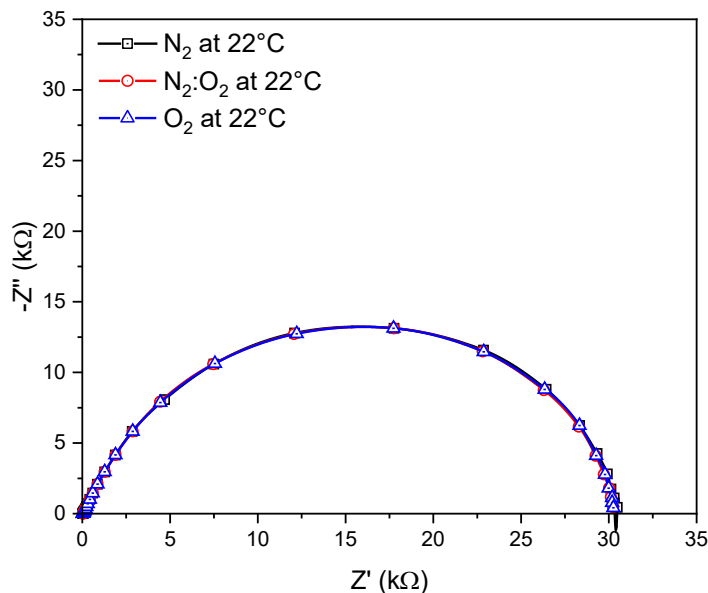


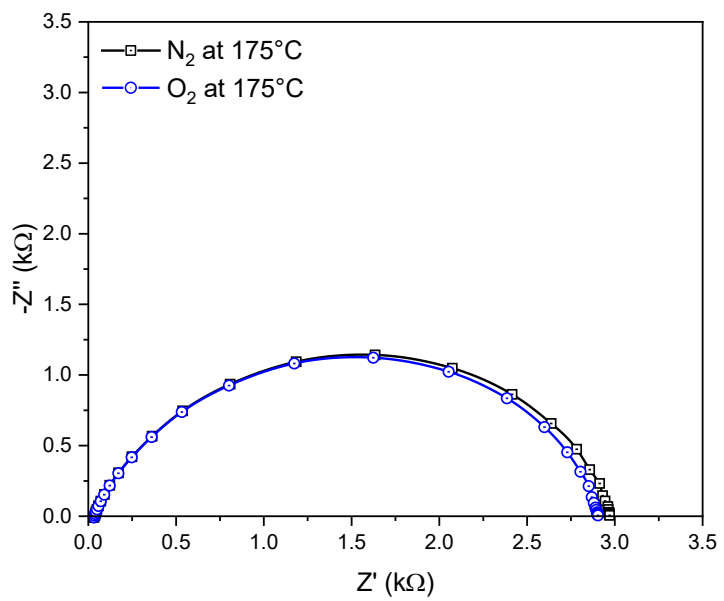
Figure S 12. (a) Change in the resistance of Pt-BTO-460 when switching from air (250 ml min^{-1}) to $2\% \text{ H}_2$ in N_2 (250 ml min^{-1}) and then back to air at 22°C . (b) Corresponding spectroscopic plots showing the change in Z'' and M'' vs. frequency for the data in Figure 12(a) during gas switching from air to $2\% \text{ H}_2$ in N_2 .

2.6 Electrochemical Impedance Spectroscopy Response in N_2 and O_2

(a)



(b)



(c)

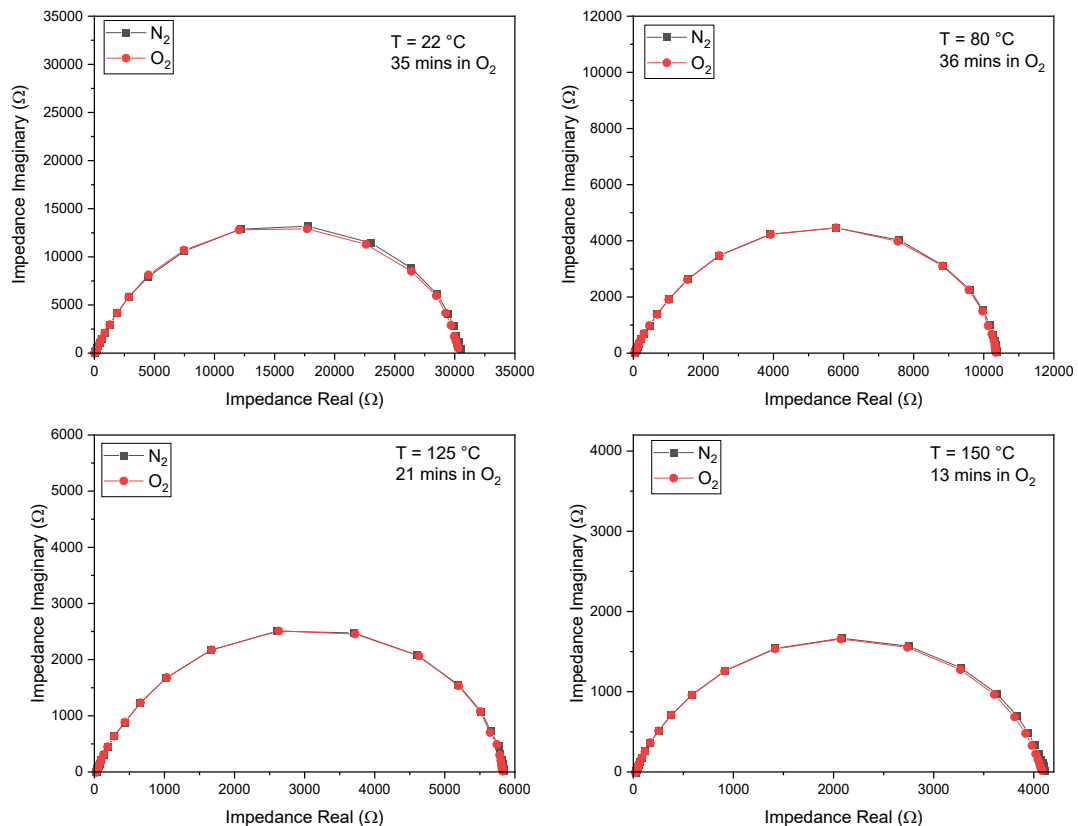


Figure S 13. Nyquist plots showing the impedance response of Pt-BTO-470 under atmospheres of (a) pure N_2 , synthetic air, and pure O_2 at $22\text{ }^{\circ}\text{C}$, (b) pure N_2 and O_2 at $175\text{ }^{\circ}\text{C}$, and (c) switching from N_2 to O_2 at $22 - 150\text{ }^{\circ}\text{C}$ and the time spent under an O_2 atmosphere .

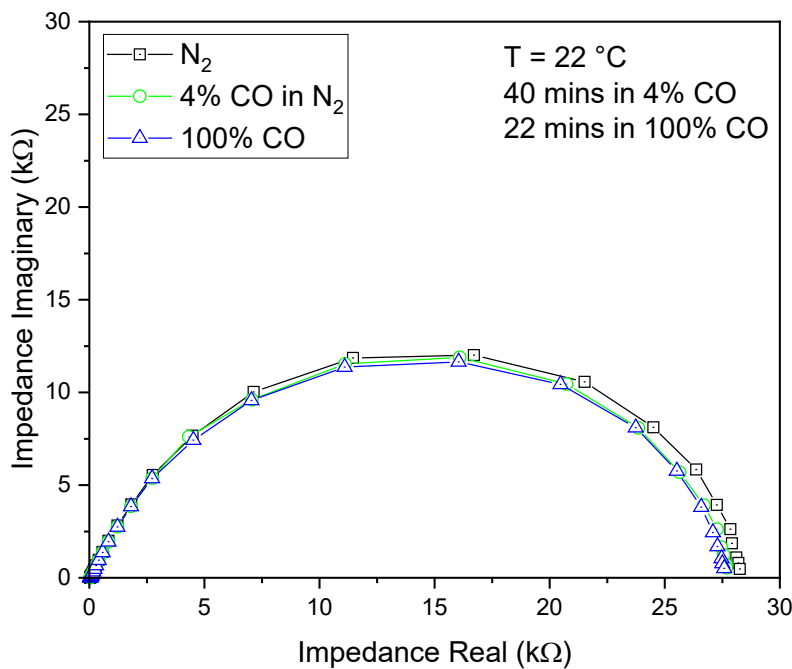


Figure S 14. Nyquist plot showing gas switching from N_2 , to 4% CO, and then to 100% CO for Pt-BTO-470 at 22 °C

2.7 Near Ambient Pressure X-Ray Photoelectron Spectroscopy (NAP-XPS)

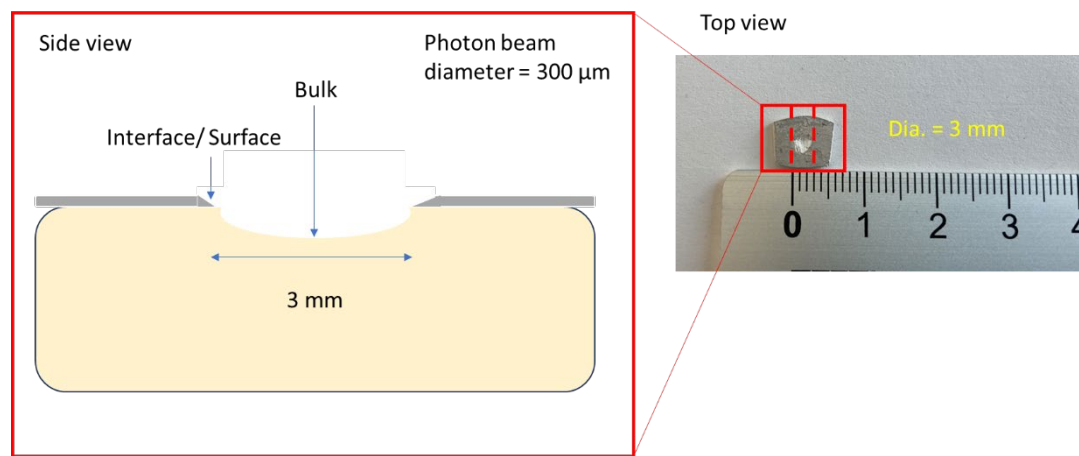


Figure S 15. Pictorial representation of the XPS measurement position at the bulk, away from the Pt-BaTiO₃ interface region. The photon beam is 300 μm in diameter, while the bulk spot is 3 mm in diameter.

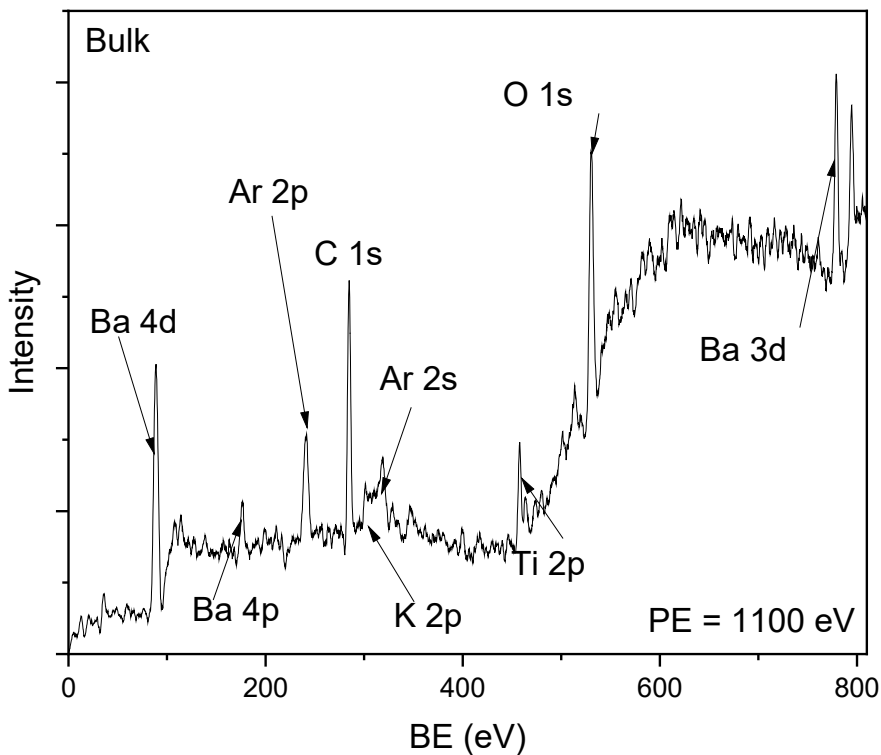


Figure S 16. Survey scan of Pt-BTO-470 at an excitation energy of 1100 eV for the bulk spot region under 1 mbar argon at 22 °C.

2.7.1 Quality Assessment of XPS Peak Fitting

The model fits to the NAP-XPS data were analysed using the Chi-squared (χ^2) and Abbe criterion to assess the quality of the model fits.¹ The Chi-squared quantity gives a measure of the goodness of fit between a set of experimental data points, $M(i)$, and the sum of the fit components/ peaks used to model that data, $S(i, \vec{p})$, where the \vec{p} vector is the set of parameters upon which the fit components depend. The Chi-squared is calculated point by point by squaring the difference between $M(i)$ and the value of the fit at the same point, $S(i, \vec{p})$. The Chi-squared values presented in the tables below are from the raw experimental data fits (after Shirley background fitting) and as reported in the XPSPEAK41 fitting software. The relative peak areas are also reported, which were calculated from the area of the i^{th} component of the core level under examination divided by the total peak envelope for that core level.

$$\chi^2(\vec{p}) = \sum_{i=1}^N \frac{[M(i) - S(i, \vec{p})]^2}{M(i)}$$

The residual is the difference between the fit and experimental data point.

$$R(i) = S(i, \vec{p}) - M(i)$$

The Abbe criterion quantifies the distribution of the residuals of the fit. For random noise and statistically distributed residuals, the Abbe criterion should be close to or equal to 1. Values close to zero indicate that the data is consistently above or below the fit. A value of 2 indicates that the residuals are anticorrelated (same magnitude but alternating sign). Hence, a value of 1 is desired for a good quality fit.

$$Abbe = \frac{\frac{1}{2} \sum_{i=1}^{N-1} [R(i+1) - R(i)]^2}{\sum_{i=1}^N [R(i)]^2}$$

2.7.2 O 1s Photoemission Peak for Pt-BTO-470

Table S 3. O 1s peak deconvolution parameters at 22 °C from 1 mbar argon to 4 mbar H₂

Gas Type and Pressure (mbar)	O 1s Components									χ^2	Abbe Criterion		
	O ²⁻ (Lattice)			OH			Adsorbed H ₂ O						
	BE (eV)	FWHM (eV)	Rel. Area (%)	BE (eV)	FWHM (eV)	Rel. Area (%)	BE (eV)	FWHM (eV)	Rel. Area (%)				
1 mbar Ar	528.9	1.3	18.9	530.7	1.9	49.9	532.5	1.7	12.2	268.5	0.77		
1 mbar H ₂	529.0	1.4	21.8	530.6	1.9	34.6	532.3	1.75	21.8	362.7	0.66		
2 mbar H ₂	529.0	1.3	14.5	530.6	1.9	29.0	532.4	1.7	41.9	360.3	0.81		
4 mbar H ₂	529.0	1.3	8.2	530.6	1.9	28.1	532.4	1.8	55.4	378.7	0.79		

Addition to Table S3 above for inclusion of a carbonate peak component to the O 1s peak fitting

Gas Type and Pressure (mbar)	BE (eV)	FWHM (eV)	Rel. Area (%)
1 mbar Ar	531.4	1.8	18.9
1 mbar H ₂	531.6	1.8	21.8
2 mbar H ₂	531.5	1.8	14.5
4 mbar H ₂	531.6	1.8	8.2

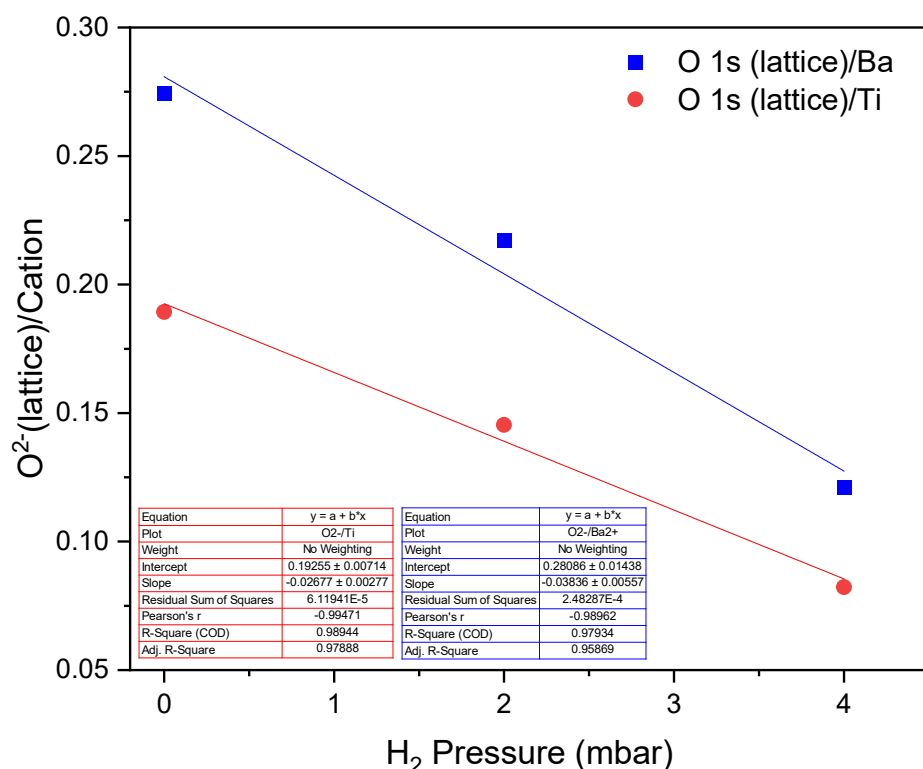
Table S 4. O 1s peak deconvolution parameters under 2 mbar H₂ and from 22 °C to 150 °C

Temperature (°C)	O 1s Components									χ^2	Abbe Criterion		
	O ²⁻ (Lattice)			OH			Adsorbed H ₂ O						
	BE (eV)	FWHM (eV)	Rel. Area (%)	BE (eV)	FWHM (eV)	Rel. Area (%)	BE (eV)	FWHM (eV)	Rel. Area (%)				
22	529.0	1.3	14.54	530.6	1.9	29.03	532.4	1.7	41.89	360.3	0.81		
80	529.0	1.3	10.83	530.6	1.9	26.94	532.4	1.8	51.41	428.7	0.63		
125	529.0	1.3	9.47	530.6	1.9	22.02	532.4	1.9	59.04	296.3	0.95		
150	529.1	1.3	10.57	503.7	1.9	20.34	532.3	1.8	58.52	306.6	0.90		

Addition to Table S4 above for inclusion of a carbonate peak component to the O 1s peak fitting

Gas Type and Pressure (mbar)	BE (eV)	FWHM (eV)	Rel. Area (%)
22	531.5	1.8	14.54
80	531.6	1.8	10.83
125	531.6	1.8	9.47
150	531.7	1.8	10.57

(a)



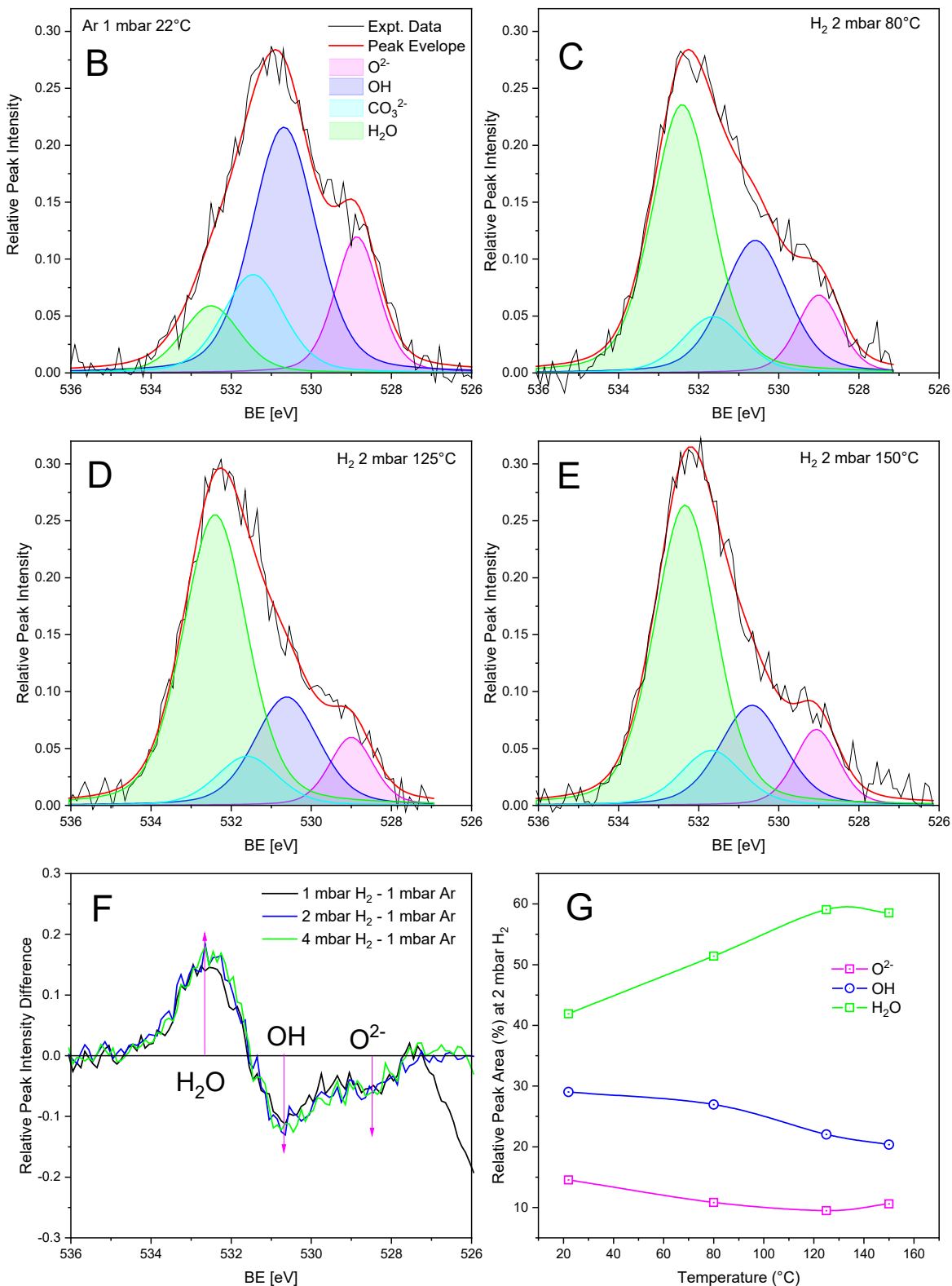


Figure S 17. a) Ratio of the lattice oxygen (O^{2-}) peak area from O 1s to the BaTiO₃ Ba 4d and Ti 2p peak areas as a function of H₂ pressure. O 1s photoemission spectra, and peak deconvolution, collected at the BaTiO₃ spot (using a photon energy of 850 eV) and under atmospheres of (b) 1 mbar argon at 22 °C, (c) 2 mbar H₂ at 80 °C (d) 2 mbar H₂ at 125 °C,

and (e) 2 mbar H₂ at 150 °C. (f) Difference spectra of the O 1s photoemission signal with increasing H₂ pressure, calculated using the 1 mbar argon spectrum as a reference. (g) Change in the O 1s relative peak areas under 2 mbar of H₂ and as a function of temperature.

2.7.3 C 1s Photoemission Peak for Pt-BTO-470

The C1s photoemission spectra for Pt-BTO-470 under 1 mbar argon and 1-4 mbar H₂ are shown in Fig S16 a-d, and the relative peak areas are shown in Table S.5. Spectra were collected using a photon energy of 850 eV and can be deconvoluted into four components centered at 282.2-283 eV, 284.8 eV, 286-287 eV, and 288-289 eV, which corresponding to Ti-C, Sp³ C-C, C-O, and CO₃²⁻ species (Fig S.16).² The adventitious carbon peak (Sp³ C-C) occupies 65-72 % (Table 5) of the relative peak envelope area. These relative areas are comparable to those found by Miot et al.² and explained by air contamination, or in our case, also due to contamination from the graphite molds during spark plasma sintering. However, the contribution of SPS contamination should be minimal as the surface was polished and underwent post-sintering oxidation to remove as much carbon as possible. The relative peak areas did not change significantly with increasing H₂ pressure, and this was confirmed by plotting the C 1s difference spectra, using the 1 mbar Ar spectrum as a reference (Fig. S16 e and f). There is a peak centered at 282 eV and this could be attributed to the presence of a titanium carbide Ti-C bond, which may have formed during spark plasma sintering.³ However, a corresponding peak should also appear in the Ti 2p spectrum at 455 eV⁴ (see below), and it is difficult to resolve this due to the high noise level, and also due to possible asymmetry at lower binding energy, of the Ti 2p photoemission spectra. Additionally, a carbonate peak is present at 288-289 eV, which increases slightly with H₂ pressure. Therefore, a carbonate peak was added to the O 1s spectra fitting to ensure reliable relative peak area determination of O²⁻, OH and adsorbed H₂O components.

Table S 5. Pt-BTO-470 Relative component areas (%) binding energies (eV), FWHM (eV), and Abbe values for C 1s XPS analysis at 22°C from 1 mbar argon to 4 mbar H₂

Gas Type and Pressure	C 1s Components (Relative Areas/ %)					χ^2	Abbe Criterion
	FWHM=1.6 282.2- 283eV	FWHM=1.9 284.8 eV	FWHM=1.6- 1.7 286-2870eV	FWHM=1.6- 1.7 288-289 eV			
	Ti-C	(Sp ³) C-C/C-H	C-O	BaCO ₃			
1 mbar Ar	10.35	66.92	9.11	13.62	315.5	0.88	
1 mbar H ₂	10.10	64.95	12.33	12.63	378.0	0.60	
2 mbar H ₂	9.06	67.88	14.92	8.14	389.7	0.69	
4 mbar H ₂	6.97	72.16	12.51	8.35	247.4	1.05	

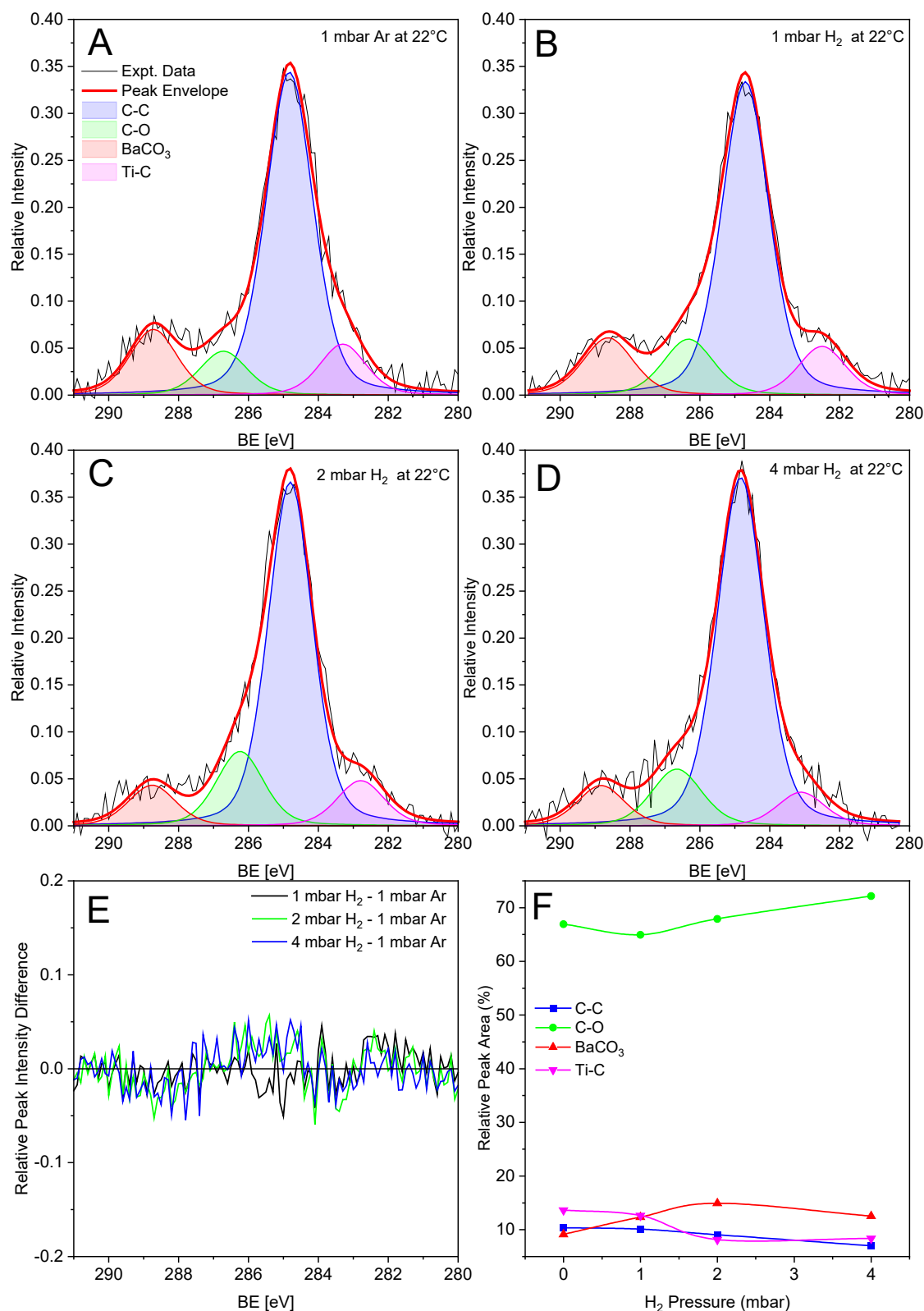


Figure S 18. C 1s photoemission spectra, and peak deconvolution, collected at 22 °C at the BaTiO_3 spot (using a photon energy of 850 eV) and under atmospheres of (a) 1 mbar argon, (b) 1 mbar H_2 , (c) 2 mbar H_2 , and (d) 4 mbar H_2 . (e) Difference spectra of the C 1s

photoemission signal with increasing H₂ pressure, calculated using the 1 mbar argon spectrum as a reference. (f) Change in the C 1s relative peak areas as a function of H₂ pressure at 22 °C.

2.7.4 Ti 2p Photoemission Peak for Pt-BTO-470

The Ti 2p photoemission spectra for Pt-BTO-470 under 1 mbar argon and 1-4 mbar H₂ are shown in Fig S17 a-d, and the relative peak areas are shown in Table S6. Spectra were collected using a photon energy of 850 eV and can be deconvoluted into one doublet component with the Ti 2p_{3/2} peak centered at a binding energy of 457.7 – 457.9 eV, which is representative of Ti⁴⁺.^{2, 5} The spin orbit splitting between Ti 2p_{3/2} and Ti 2p_{1/2} peak is between 5.7 to 5.8 eV, which is consistent with values in the literature.⁵ The Ti-C peak observed in the C 1s photoemission spectra is not observed in the Ti 2p spectra, which should appear at 455 eV; however, the noise level of this data set is high and is difficult to deconvolute the spectra into additional peaks. There was no obvious change in relative peak intensity with increasing H₂ pressure demonstrating that titanium related surface states remained constant. Ti³⁺ may be present at lower binding energies (457 eV) but it is difficult to resolve this due to the high spectral noise level.

Table S 6. Ti 2p peak fitting parameters at 22 °C and from 1 mbar argon to 4 mbar H₂

Gas Type and Pressure	Ti 2p Components				
	Ti 2p _{3/2} Peak Binding Energy (eV)	SOS	FWHM	χ^2	Abbe Criterion
1 mbar Ar	457.67	5.7	1.4	497.2	0.54
1 mbar H ₂	457.74	5.8	1.4	437.8	0.50
2 mbar H ₂	457.91	5.7	1.4	320.1	0.77
4 mbar H ₂	457.94	5.7	1.4	344.5	0.74

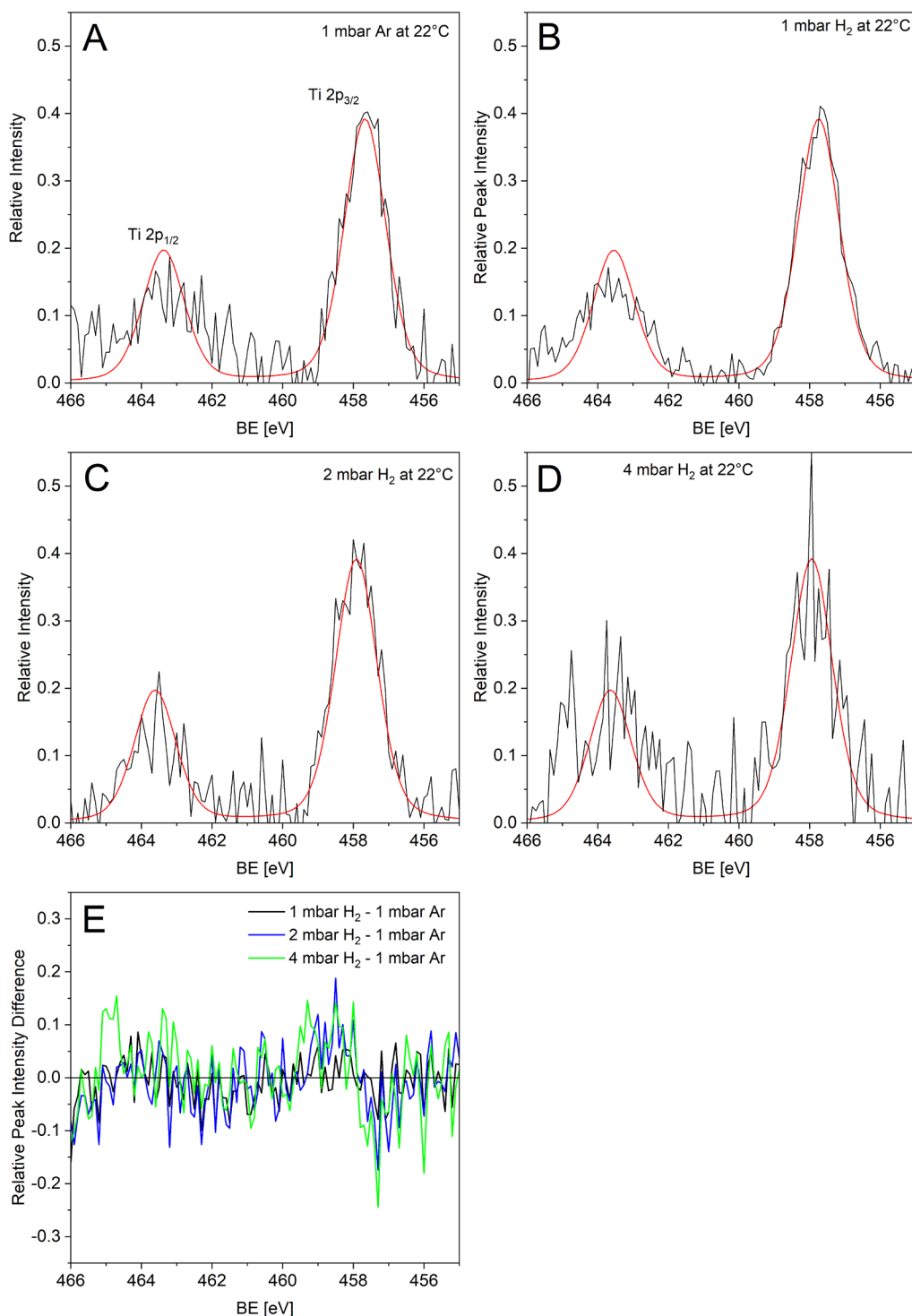


Figure S 19. Ti 2p photoemission spectra, and peak fitting, collected at 22 °C at the Ba-TiO₃ spot (using a photon energy of 850 eV) and under atmospheres of (a) 1 mbar argon, (b) 1 mbar H₂, (c) 2 mbar H₂, and (d) 4 mbar H₂. (e) Difference spectra of the Ti 2p photoemission signal with increasing H₂ pressure, calculated using the 1 mbar argon spectrum as a reference.

2.7.5 Ba 4d Photoemission Peak for Pt-BTO-470

The Ba 4d photoemission spectra for Pt-BTO-470 under 1 mbar argon and 1-4 mbar H₂ are shown in Fig S18 a-d, and the relative peak areas are shown in Table S7. Spectra were collected using a photon energy of 850 eV and can be deconvoluted into two doublet components with the Ba 4d_{3/2} peak centered at 87.7 – 90.3 eV due to BaTiO₃, and at 89 – 91.8 eV due to BaCO₃.^{2, 5} There is no change in the Ba 4d relative peak areas with H₂ concentration, which exhibit a constant BaTiO₃ to BaCO₃ ratio of 70:30. This suggests that carbonates are stable and do not react with hydrogen at 22 °C.

Table S 7. Ba 4d peak fitting parameters at 22 °C and from 1 mbar argon to 4 mbar H₂

Gas Type and Pressure	Ba 4d Components					χ^2	Abbe Criterion		
	Peak 1 - BaTiO ₃		Peak 2 - BaCO ₃						
	Binding Energy (eV)	Rel. Area	Binding Energy (eV)	Rel. Area					
1 mbar Ar	87.75	0.69	89.11	0.31	565.0	0.66			
1 mbar H ₂	87.80	0.68	89.14	0.32	615.7	0.50			
2 mbar H ₂	87.97	0.67	89.27	0.33	447.4	0.93			
4 mbar H ₂	88.04	0.68	89.30	0.32	379.0	0.83			

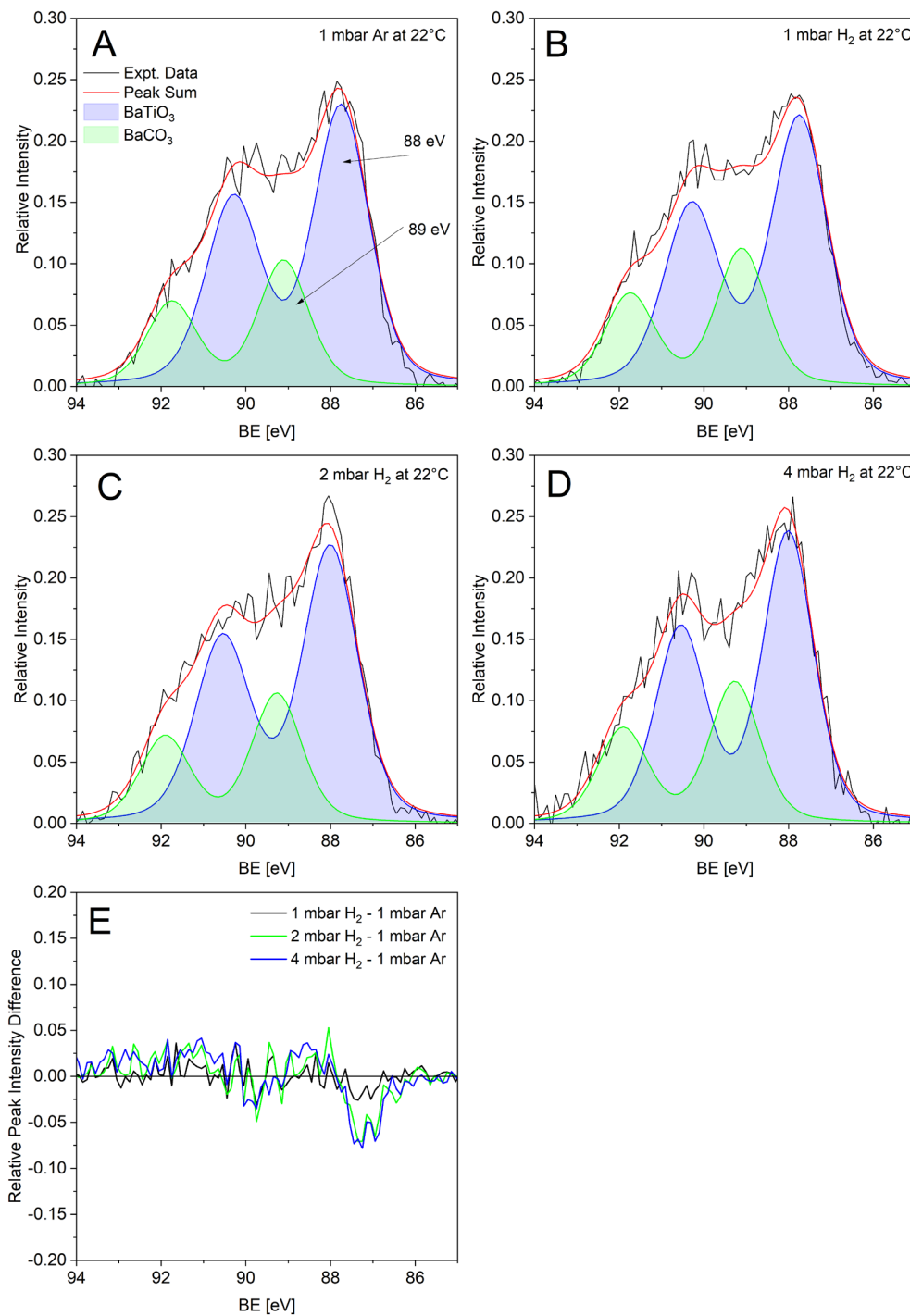


Figure S 20. Ba 4d photoemission spectra, and peak deconvolution, collected at 22 °C at the BaTiO₃ spot (using a photon energy of 850 eV) and under atmospheres of (a) 1 mbar argon, (b) 1 mbar H₂, (c) 2 mbar H₂, and (d) 4 mbar H₂. (e) Difference spectra of the Ba 4d photoemission signal with increasing H₂ pressure, calculated using the 1 mbar argon spectrum as a reference.

2.7.6 Pt 4f Photoemission Peak for Pt-BTO-470

The Pt-BaTiO₃ interface region was also studied by XPS to measure the Pt 4f spectrum as a function of H₂ pressure. This was performed to determine the presence of elemental Pt (71 eV) as well as the possible formation of oxides (74 – 75 eV) and hydroxides (73 – 74 eV).⁵ The platinum XPS measurements were recorded at a different location to the C 1s, O 1s, Ti 2p, and Ba 4d spectra (which were collected at a pure BaTiO₃ spot where the platinum was removed). The peak fitting parameters for the Pt 4f core level are shown in Table S8 below. The Pt doublet 4f_{7/2} peak is centred at approximately 71 eV, which is typical for elemental platinum with a spin orbit splitting of 3.33 eV, as reported in the literature.⁵ There was no indication of the formation of Pt oxides or hydroxides and there was no change in the Pt 4f spectral intensity with increasing H₂ pressure, as shown in Fig. S.19 a-e.

Table S 8. Pt 4f peak fitting parameters at 22 °C and from 1 mbar argon to 4 mbar H₂ for the BaTiO₃-Pt interface region.

Gas Type and Pressure	Pt 4f Components			
	Pt 4f _{7/2} Peak Binding Energy (eV)	FWHM	χ^2	Abbe Criterion
1 mbar Ar	70.8	1.08	420.4	0.82
1 mbar H ₂	70.8	1.08	816.3	1.00
2 mbar H ₂	70.8	1.08	350.8	0.93
4 mbar H ₂	70.8	1.08	351.8	1.23

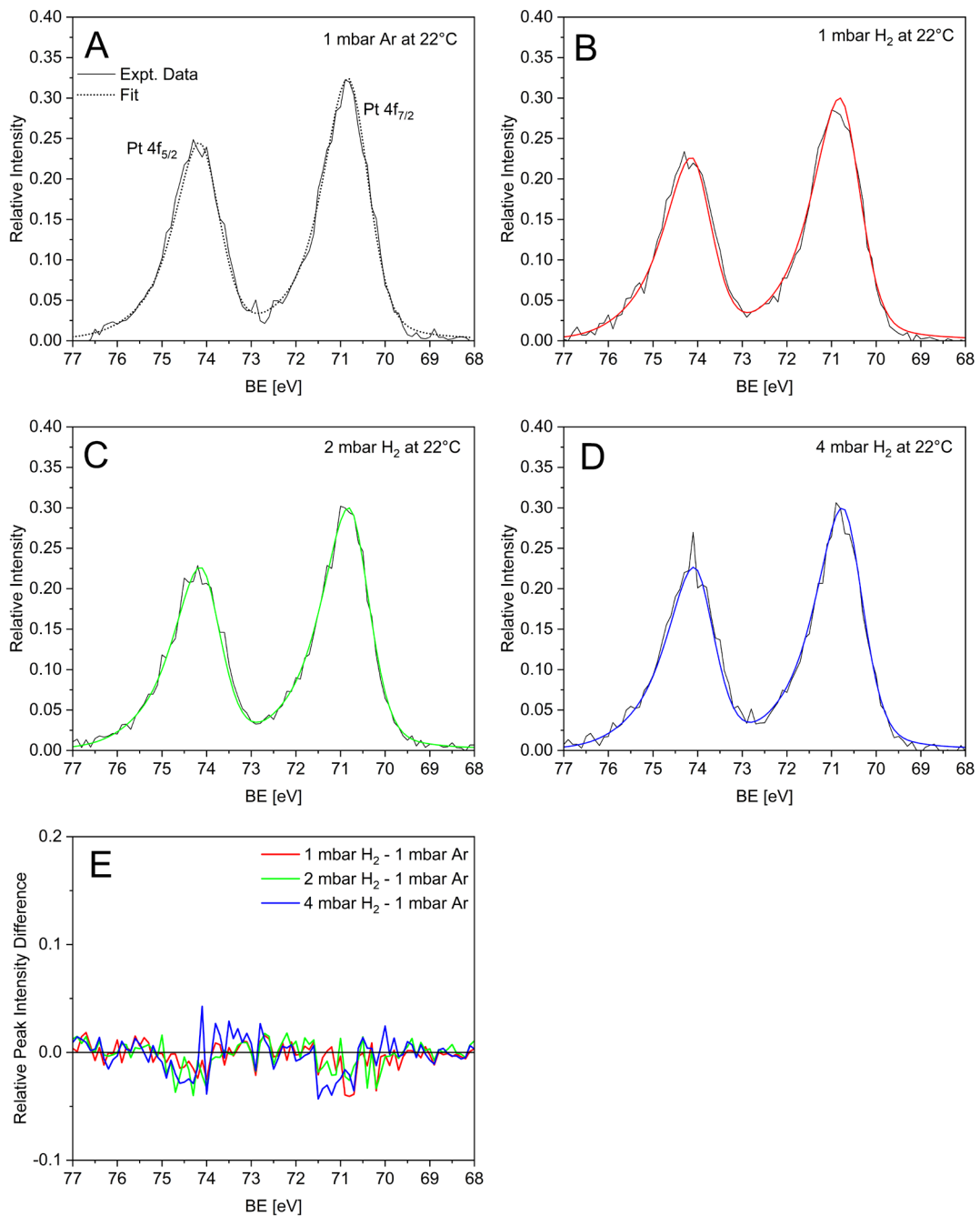


Figure S 21. Pt 4f photoemission spectra, and peak fitting, collected at 22 °C at the Ba-TiO₃-Pt interface region (using a photon energy of 850 eV) and under atmospheres of (a) 1 mbar argon, (b) 1 mbar H₂, (c) 2 mbar H₂, and (d) 4 mbar H₂. (e) Difference spectra of the Pt 4d photoemission signal with increasing H₂ pressure, calculated using the 1 mbar argon spectrum as a reference.

2.8 Electrochemical Impedance Spectroscopy Studies

2.8.1 H₂ and D₂ Kinetic isotope Studies at 22 °C and 130 °C

Table S 9. Pt-BTO-470 conductivities in H₂ and D₂ at 22 °C and 130 °C and the corresponding D₂ and H₂ conductivity ratios

Temperature (°C)	Molar Flow Rate ($\times 10^{-3}$ mol min ⁻¹)	Cond. in D ₂ ($\times 10^{-6}$ S cm ⁻¹)	Cond. in H ₂ ($\times 10^{-6}$ S cm ⁻¹)	D/ H
22	0	2.91	2.77	1.05
22	0.35	12.94	12.09	1.07
22	0.92	14.56	13.91	1.05
22	2.60	15.76	14.96	1.05
130	0	14.31	13.40	1.07
130	0.35	116.66	107.76	1.08
130	0.92	147.96	140.26	1.05
130	2.60	177.54	176.84	1.00

a)

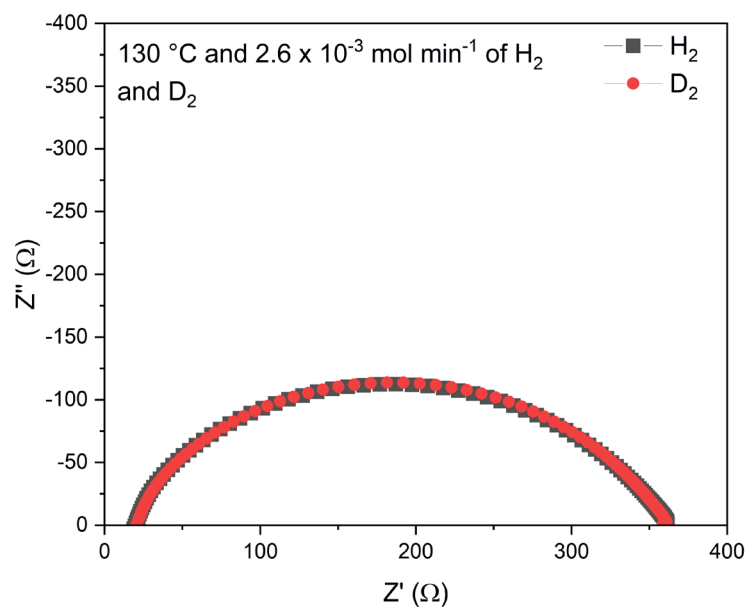


Figure S 22. (a) Nyquist plot for Pt-BTO-470 under a molar flow rate 2.6×10^{-3} mol min⁻¹ of H₂ and D₂ at 130 °C.

2.8.2 AC Conductivity Analysis: Jonscher Analysis as a Function of H₂ Concentration and Temperature

Table S 10. Jonscher model fit parameters (DC conductivity, A, and S) values for Pt-BTO-470 at 22 °C

H ₂ Concentration (%)	dc conductivity ($\sigma_{dc}/x 10^{-6} \text{ S cm}^{-1}$)	A ($x 10^{-8}$)	A error ($x 10^{-9}$)	S	S error ($x 10^{-3}$)	R ²
0	2.11	1.97	1.33	0.73	4.56	0.9984
0.4	9.61	2.21	1.92	0.74	5.91	0.9974
1.04	12.3	2.31	1.99	0.73	5.86	0.9974
2.86	13.3	0.69	0.61	0.80	5.90	0.9978
4.63	14.0	0.64	0.58	0.81	6.05	0.9978
6.33	14.3	0.62	0.56	0.81	6.09	0.9977
7.97	14.4	0.49	0.44	0.83	5.99	0.9979
19.16	14.7	0.56	0.51	0.82	6.11	0.9977

Table S 11. Jonscher model fit parameters (DC conductivity, A, and S) values for Pt-BTO-470 at 80 °C

H ₂ Concentration (%)	dc conductivity ($\sigma_{dc}/x 10^{-6} \text{ S cm}^{-1}$)	A ($x 10^{-9}$)	A error ($x 10^{-11}$)	S	S error ($x 10^{-3}$)	R ²
0	6.18	1.02	4.02	0.93	2.75	0.9997
0.4	43.5	0.78	6.28	0.98	5.57	0.9988
1.04	47.0	0.71	5.89	0.99	5.76	0.9987
2.86	52.4	0.65	5.49	1.00	5.91	0.9987
4.63	55.0	0.61	5.21	1.00	5.95	0.9987
6.33	56.4	0.60	5.19	1.00	6.01	0.9986
7.97	58.8	0.41	4.32	1.02	7.33	0.9981
19.16	60.7	0.39	4.17	1.02	7.29	0.9981

Table S 12. Jonscher model fit parameters (DC conductivity, A, and S) values for Pt-BTO-470 at 100 °C

H ₂ Concentration (%)	dc conductivity ($\sigma_{dc}/x\ 10^{-6}\ S\ cm^{-1}$)	A (x 10 ⁻⁹)	A error (x 10 ⁻¹¹)	S	S error (x 10 ⁻³)	R ²
0	8.67	1.80	19.0	0.90	7.16	0.9975
0.4	93.06	0.80	7.7	0.99	6.62	0.9983
1.04	127.5	0.84	8.1	0.99	6.56	0.9983
2.86	139.4	0.82	7.6	0.99	6.34	0.9984
4.63	155.6	0.61	4.4	1.01	4.94	0.9991
6.33	165.6	0.96	8.8	0.98	6.29	0.9984
7.97	172.5	0.97	8.9	0.98	6.27	0.9984
19.16	178.8	0.97	8.9	0.98	6.28	0.9984

Table S 13. Jonscher model fit parameters (DC conductivity, A, and S) values for Pt-BTO-470 at 125 °C

H ₂ Concentration (%)	dc conductivity ($\sigma_{dc}/x\ 10^{-6}\ S\ cm^{-1}$)	A (x 10 ⁻⁹)	A error (x 10 ⁻¹¹)	S	S error (x 10 ⁻³)	R ²
0	10.91	3.10	33.3	0.89	7.38	0.9973
0.4	179.1	0.56	4.0	1.05	5.00	0.9992
1.04	215.9	0.69	4.9	1.04	4.99	0.9991
2.86	268.8	2.28	14.7	0.95	4.48	0.9991
4.63	340.6	3.23	21.0	0.92	4.53	0.9991
6.33	373.9	3.63	22.9	0.92	4.40	0.9991
7.97	398.0	3.29	17.3	0.92	3.69	0.9994
19.16	420.1	3.34	16.6	0.92	3.48	0.9995

Table S 14. Jonscher model fit parameters (DC conductivity, A, and S) values for Pt-BTO-470 at 150 °C

H ₂ Concentration (%)	dc conductivity ($\sigma_{dc}/x\ 10^{-6}\ S\ cm^{-1}$)	A (x 10 ⁻⁹)	A error (x 10 ⁻¹¹)	S	S error (x 10 ⁻³)	R ²
0	15.7	4.28	49.6	0.88	7.94	0.9968
0.4	284.4	1.36	10.9	0.98	5.57	0.9988
1.04	468.8	2.87	17.6	0.94	4.28	0.9992
2.86	557.9	3.60	21.1	0.92	4.11	0.9992
4.63	604.0	3.9	23.4	0.92	4.17	0.9992
6.33	619.3	2.72	11.9	0.94	3.09	0.9996
7.97	642.5	3.13	13.5	0.93	3.04	0.9996
19.16	649.9	3.19	14.0	0.93	3.10	0.9996

Table S 15. Jonscher model fit parameters (DC conductivity, A, and S) values for Pt-BTO-470 at 175 °C

H ₂ Concentration (%)	dc conductivity ($\sigma_{dc}/x 10^{-6} \text{ S cm}^{-1}$)	A ($x 10^{-9}$)	A error ($x 10^{-11}$)	S	S error ($x 10^{-3}$)	R ²
0	19.1	4.61	50.5	0.85	7.58	0.9969
0.4	683.3	4.27	18.4	0.91	3.05	0.9996
1.04	785.4	4.51	21.1	0.91	3.31	0.9995
2.86	925.9	4.95	28.5	0.90	4.07	0.9992
4.63	1030.0	5.19	34.5	0.90	4.69	0.9990
6.33	1080.0	5.88	39.7	0.89	4.78	0.9989
7.97	1110.0	5.05	36.9	0.90	5.18	0.9987
19.16	1140.0	4.93	36.2	0.90	5.19	0.9987

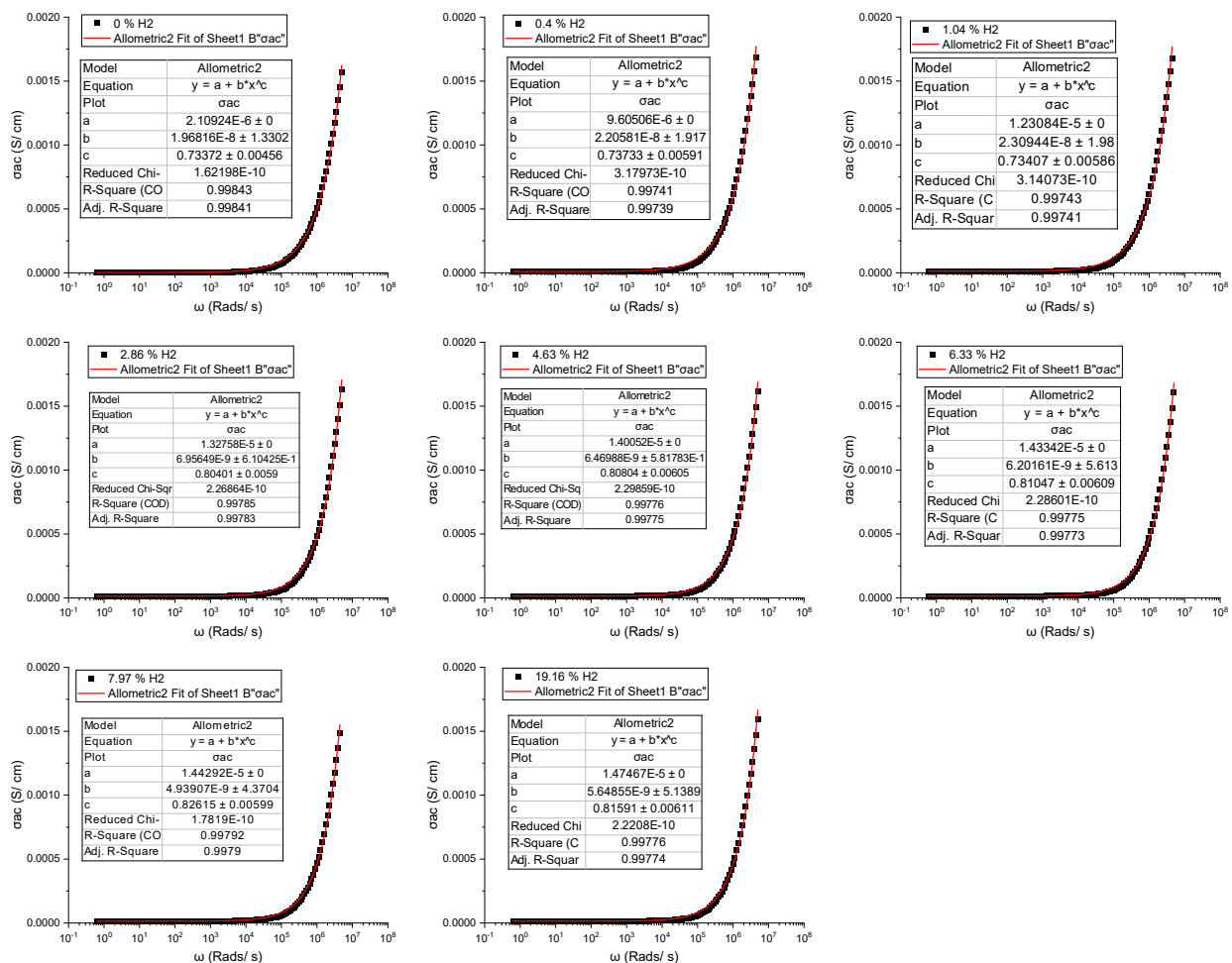


Figure S 23. Jonscher model fits to AC conductivity data for Pt-BTO-470 at 22 °C for 0% to 19% H₂ in N₂.

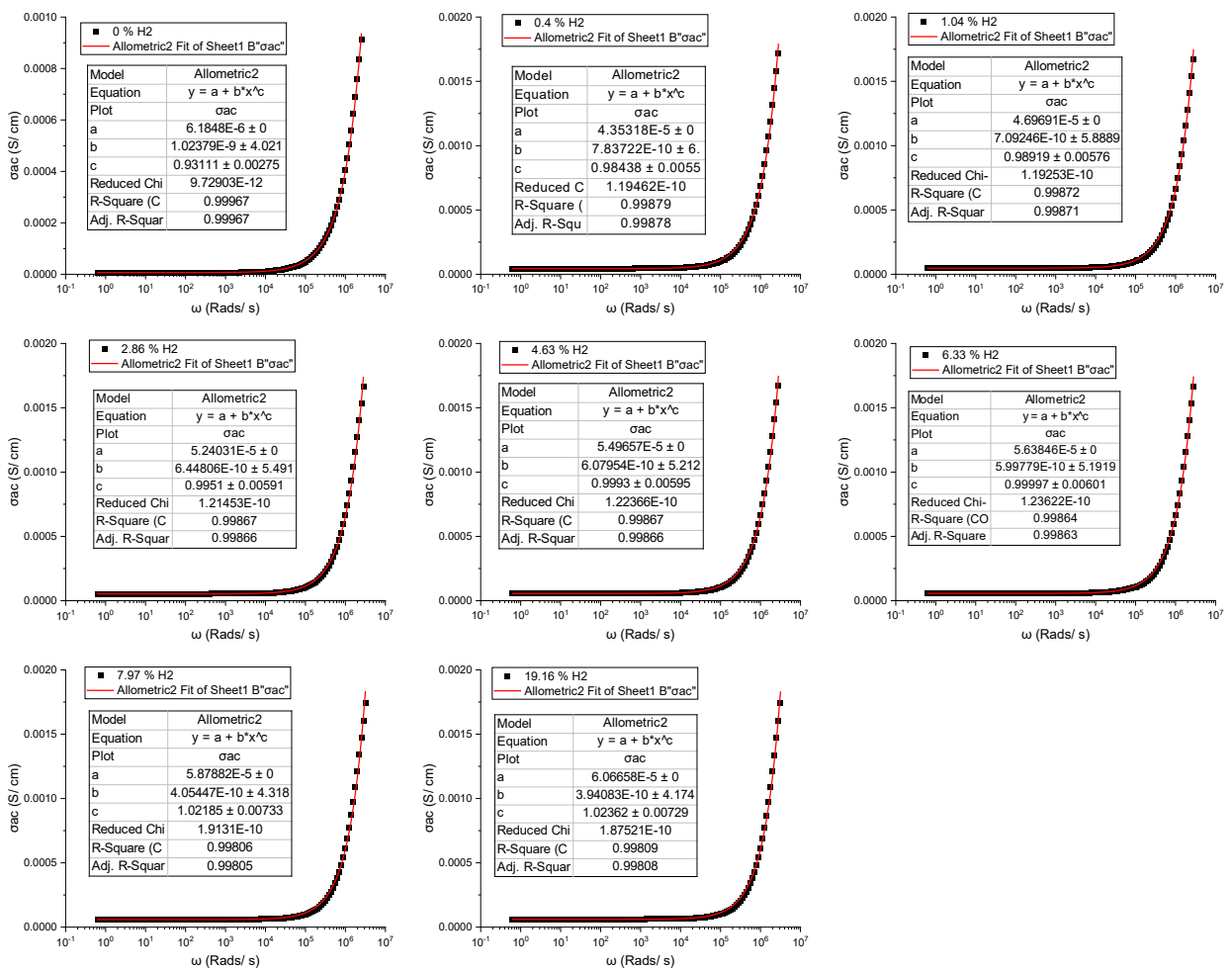


Figure S 24. Jonscher model fits to AC conductivity data for Pt-BTO-470 at 80 °C for 0% to 19% H₂ in N₂.

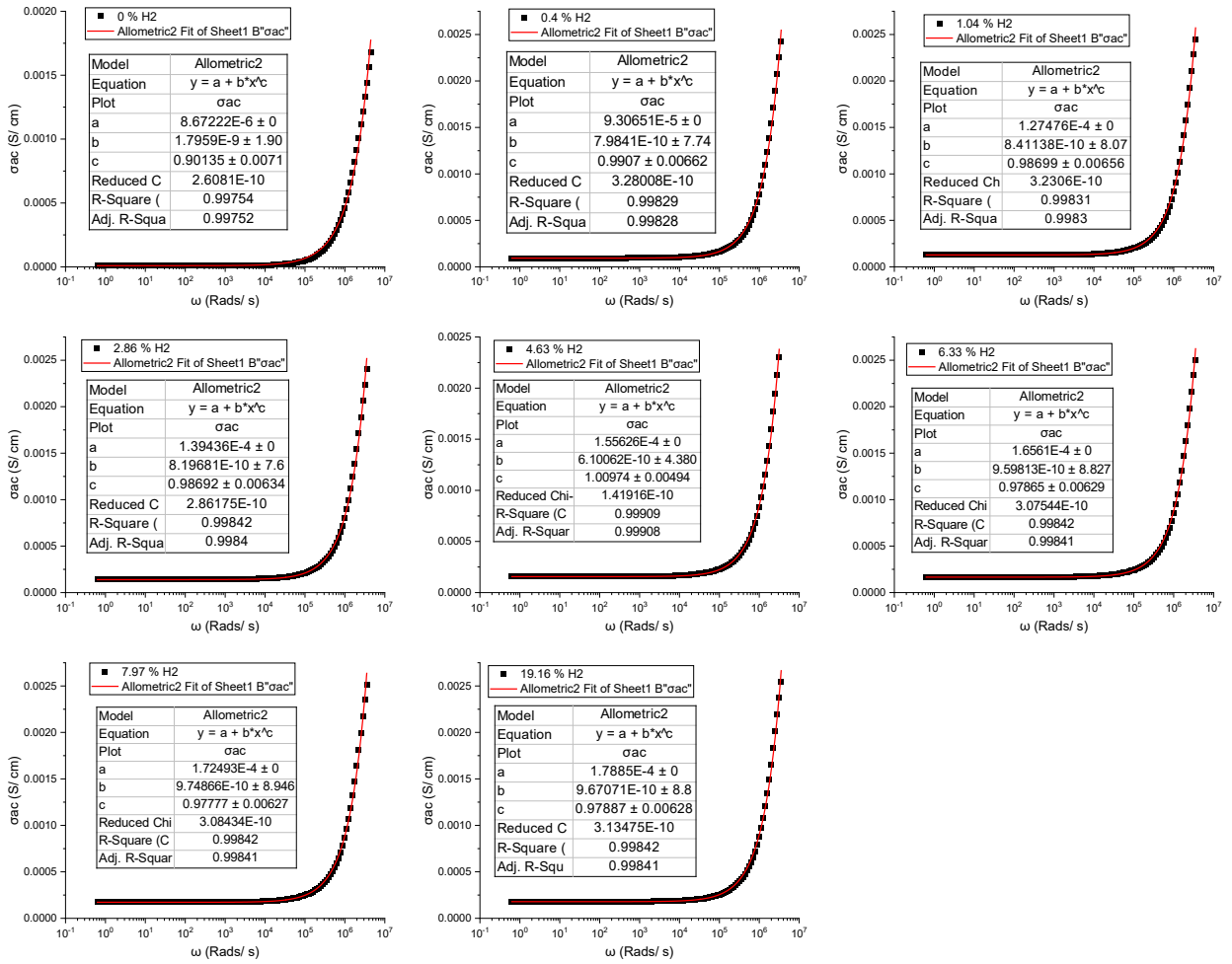


Figure S 25. Jonscher model fits to AC conductivity data for Pt-BTO-470 at 100 °C for 0% to 19% H₂ in N₂.

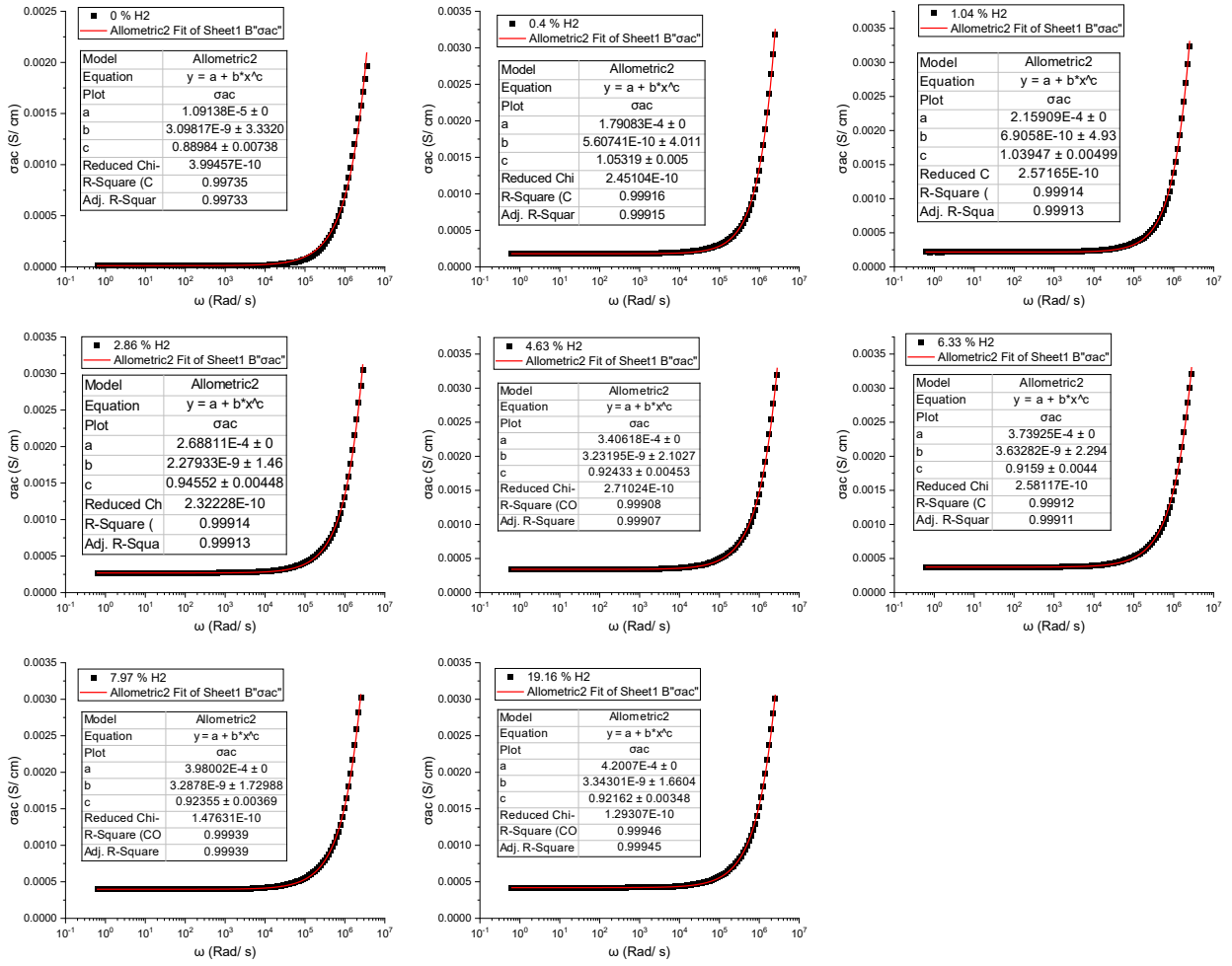


Figure S 26. Jonscher model fits to AC conductivity data for Pt-BTO-470 at 125 °C for 0% to 19% H₂ in N₂.

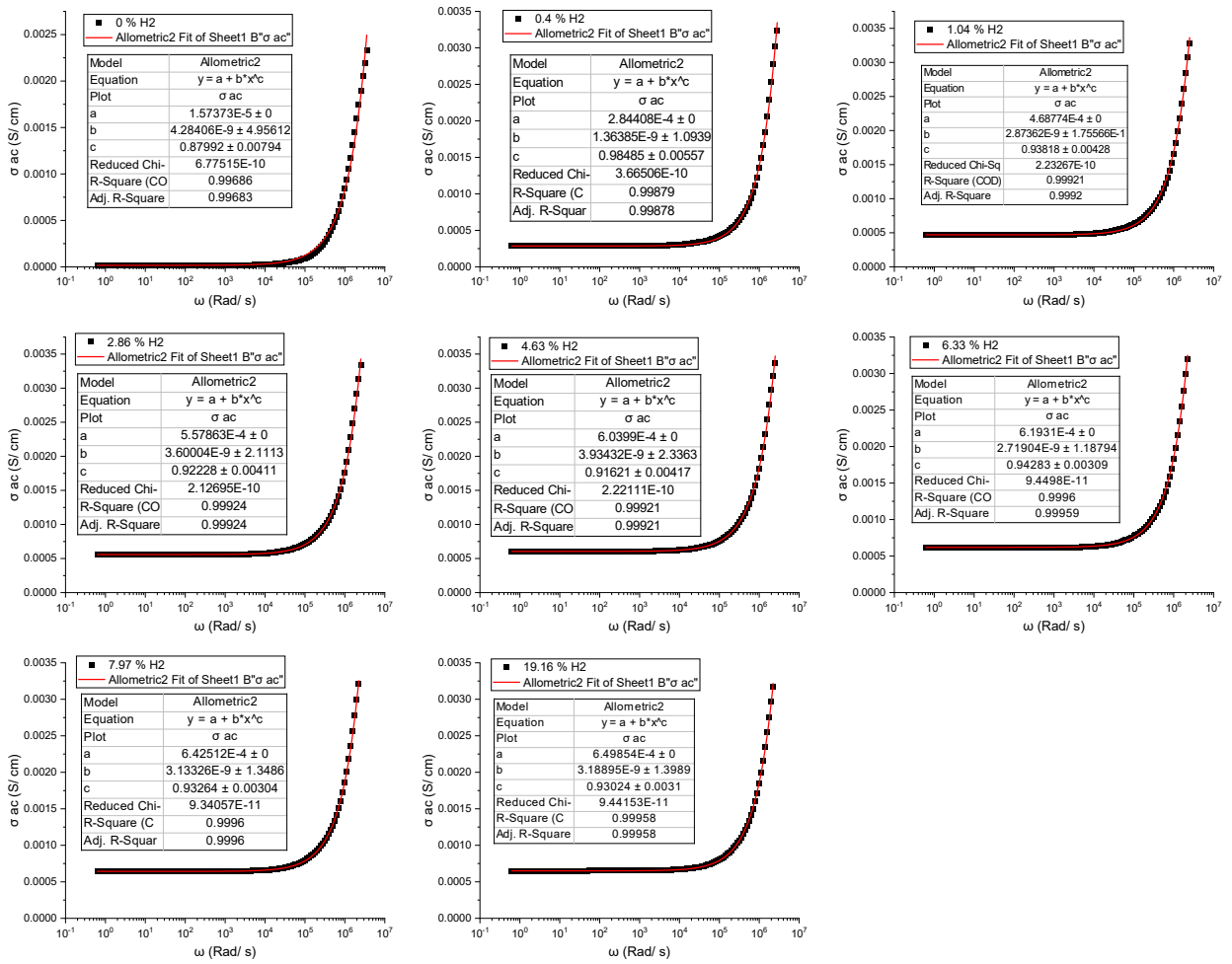


Figure S 27. Jonscher model fits to AC conductivity data for Pt-BTO-470 at 150 °C for 0% to 19% H₂ in N₂.

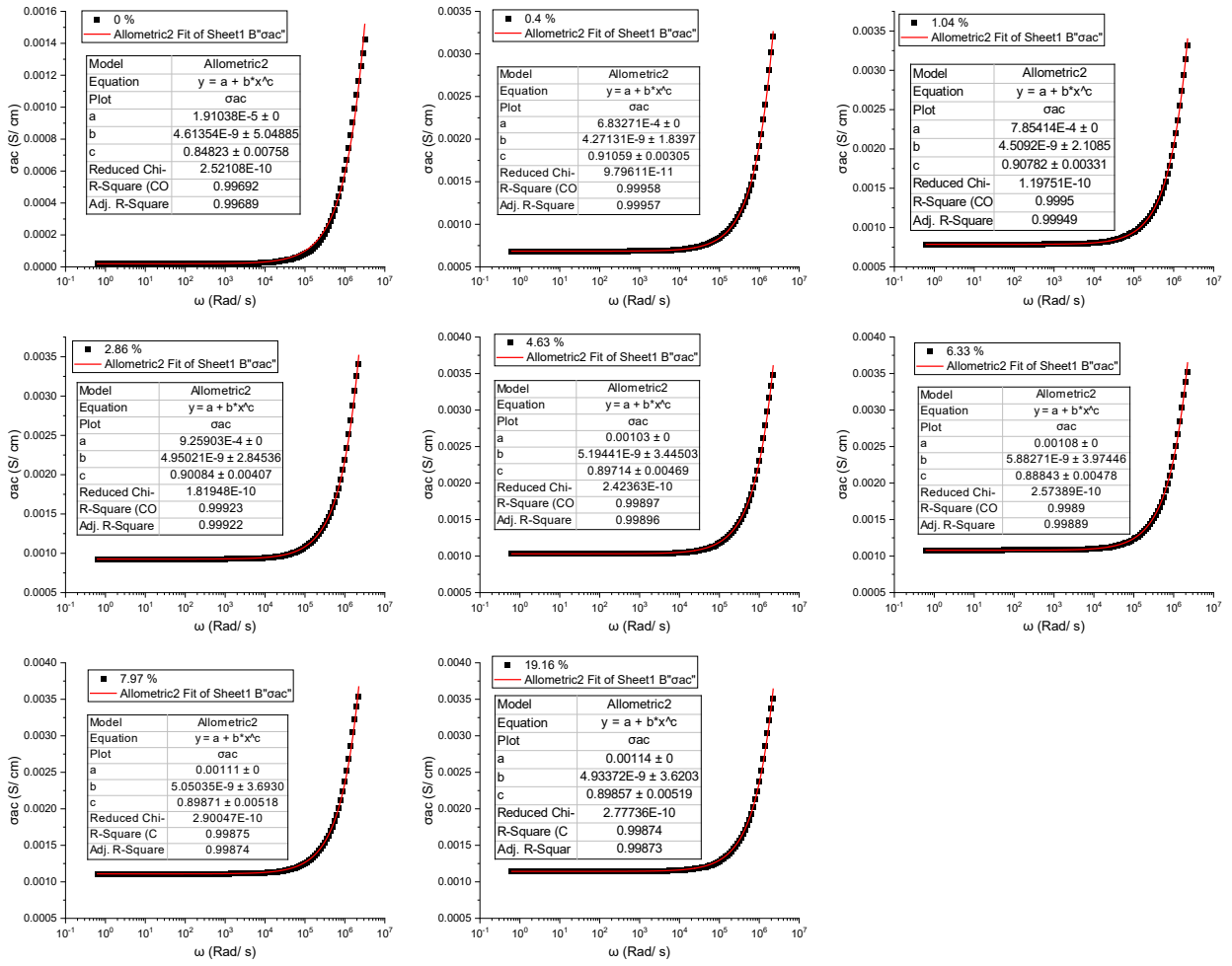


Figure S 28. Jonscher model fit to AC conductivity data for Pt-BTO-470 at 175 °C for 0% to 19% H₂ in N₂.

2.8.3 Langmuir Conductivity Model

Table S 16. Parameters derived from fitting of the Langmuir conductivity model: conductivity at 0% H₂ concentration, the parameter (A), and the Langmuir equilibrium constant (K_{eq}).

T (°C)	T (K)	1000/ T	A (x 10 ⁻⁵ S cm ⁻¹)	K (Atm ⁻¹)	ln(K)	R ²
22	295.15	3.388	1.91	83.34	4.42	0.95064
80	353.15	2.832	7.27	114.62	4.74	0.97657
100	373.15	2.680	24.68	11.80	2.47	0.98598
125	398.15	2.512	99.77	0.31	-1.18	0.97271
150	423.15	2.363	94.54	8.48	2.14	0.96154
175	448.15	2.231	146.00	20.25	3.01	0.99423

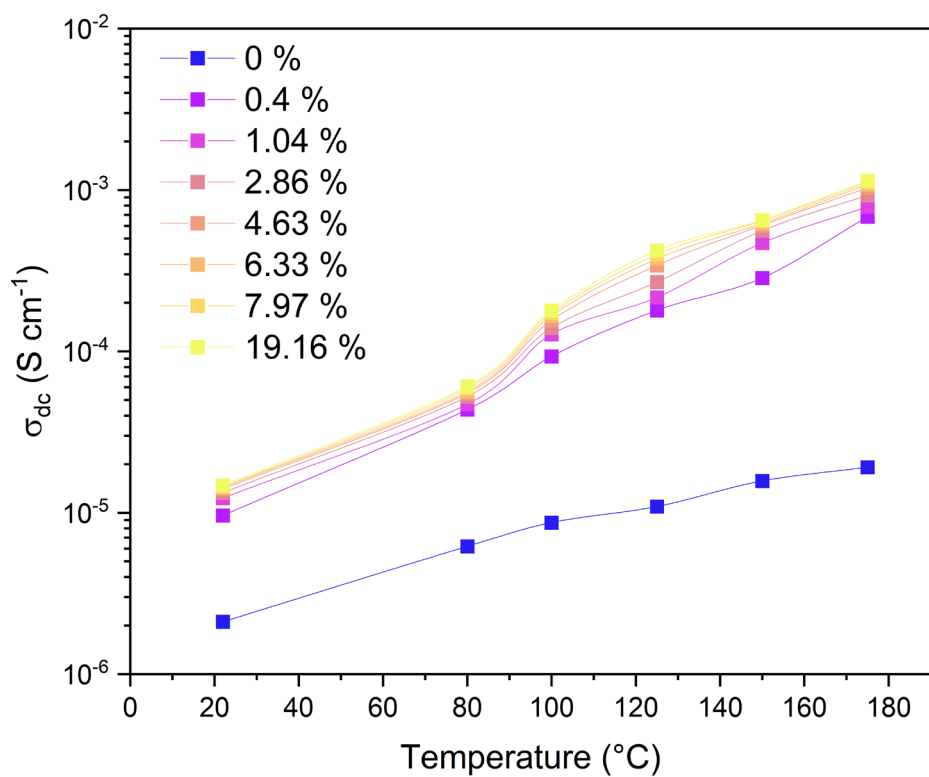


Figure S 29. Plot of DC conductivity (derived from Jonscher fit) vs. temperature for Pt-BTO-470 for 0% to 19% H₂ in N₂.

2.8.4 Charge Transport Mechanism from Jonscher Model S Parameter (S vs. T)

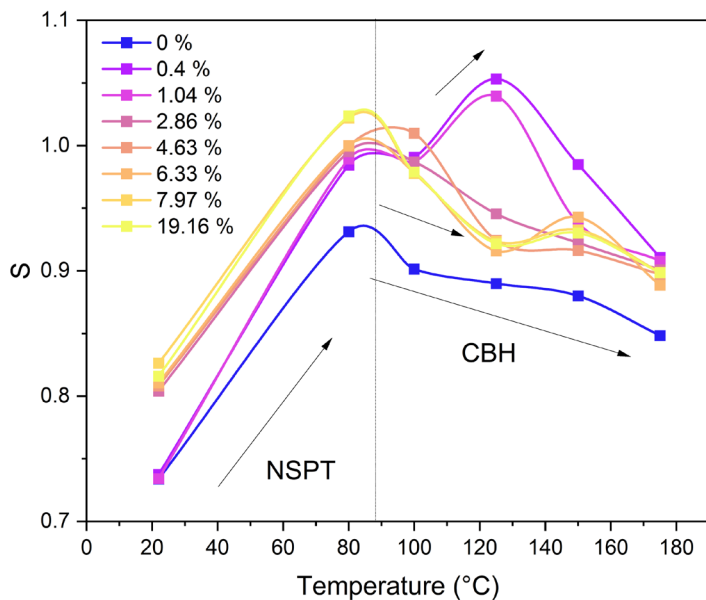


Figure S 30. Plot of Jonscher model S exponent vs. the measurement temperature (°C) and for $\text{H}_2 + \text{N}_2$ mixtures from 0 to 19% H_2 for Pt-BTO-470. Below 80 °C, the non-overlapping small polaron tunnelling model (NSPT) is the dominant charge transport mechanism, while above 80 °C, this changes to a mixture of correlated barrier hopping (CBT) and small polaron transport (NSPT) depending on the H_2 concentration. This change coincides with the ferroelectric to paraelectric phase transition temperature region for spark plasma sintered BaTiO_3 .

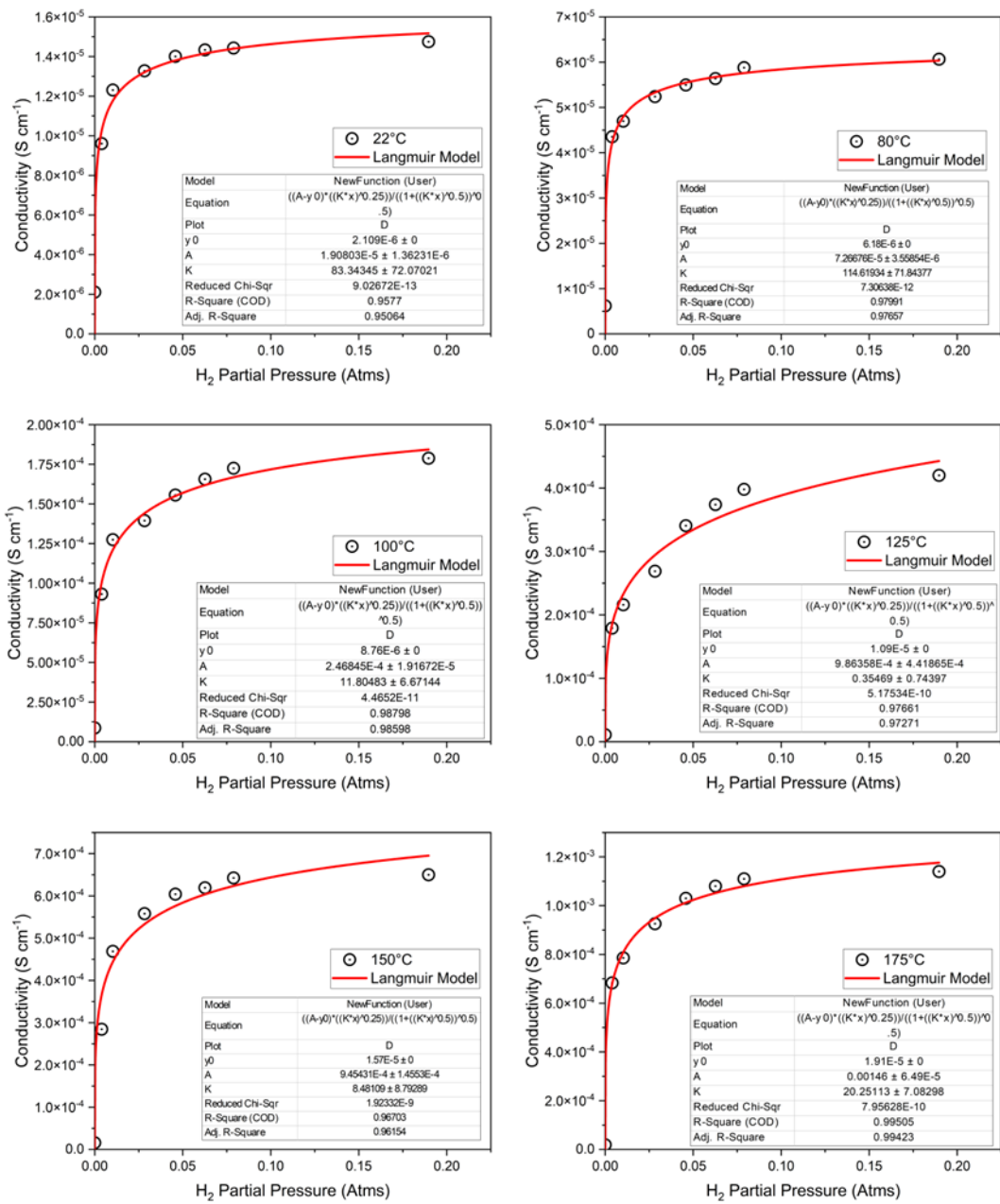


Figure S 31. Plots of conductivity (S cm⁻¹) vs. H₂ pressure (Atms) for Pt-BTO-470 for electrical measurements performed at 22 °C, 80 °C, 100 °C, 125 °C, 150 °C, and 175 °C, and fitting of Langmuir conductivity model to experimental data. Fitting parameters and statistics are shown as insets.

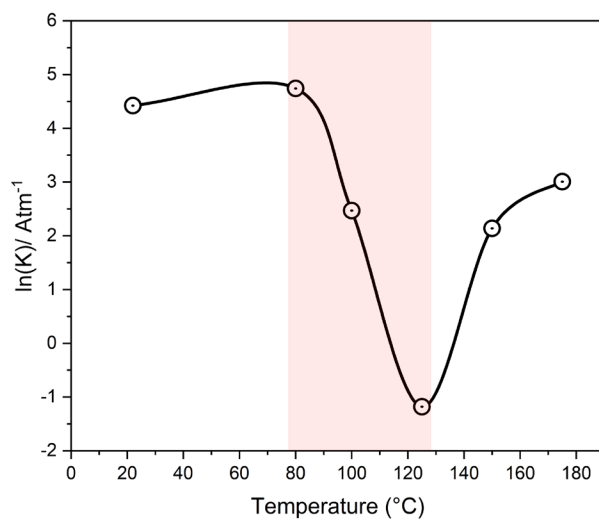


Figure S 32. Plot of the Langmuir equilibrium constant (K_{eq}) derived from Langmuir model fitting vs. the impedance measurement temperature. Plot shows a decrease in K_{eq} in the BaTiO_3 Curie temperature (T_C) region ($100 - 120$ °C).

2.8.5 Capacitance Measurements and Colossal Relative Permittivity (ϵ_r)

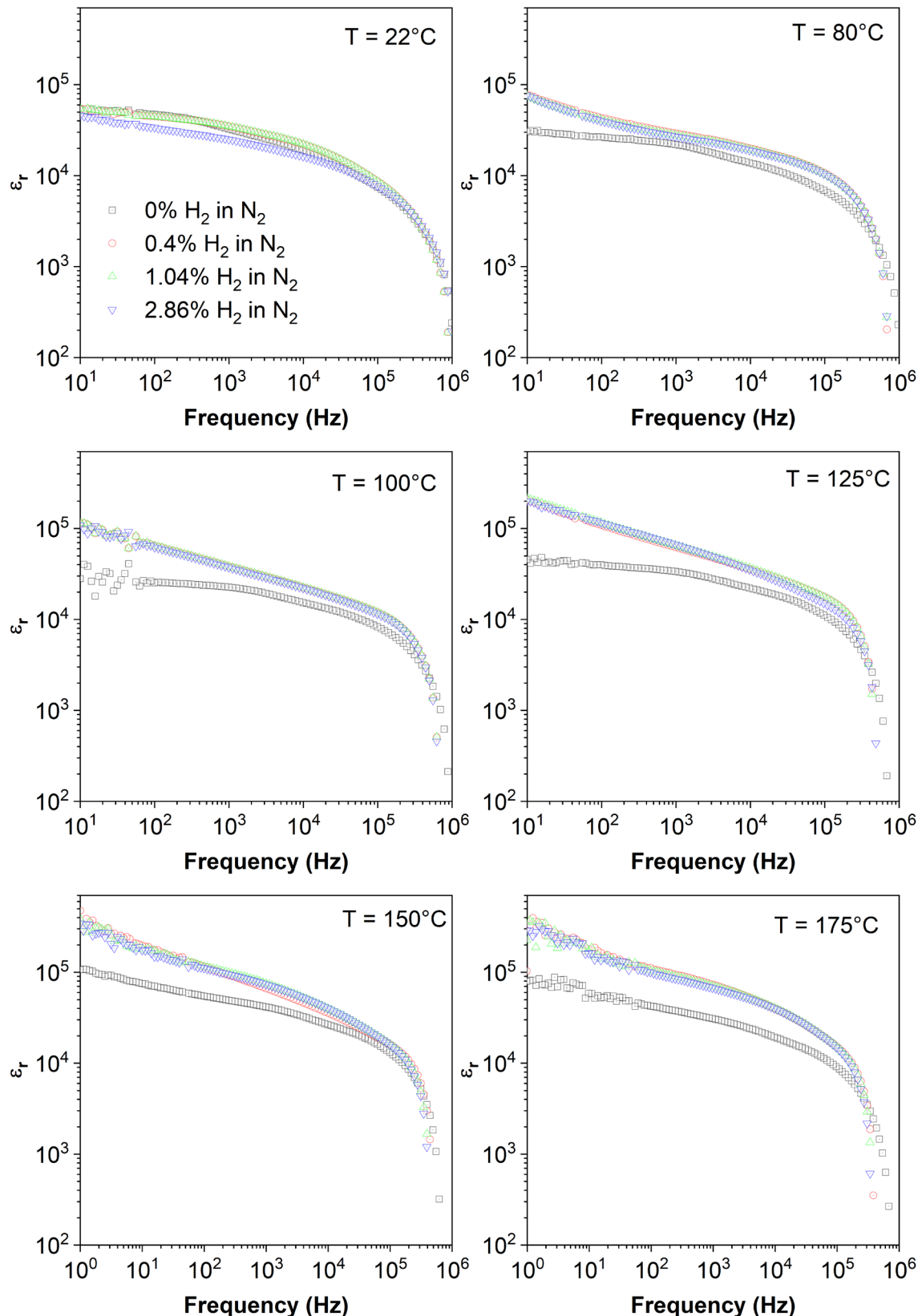


Figure S 33. Relative permittivity vs. frequency for increasing H_2 concentration (0 – 2.9%) and from 22°C to 175°C for Pt-BTO-470

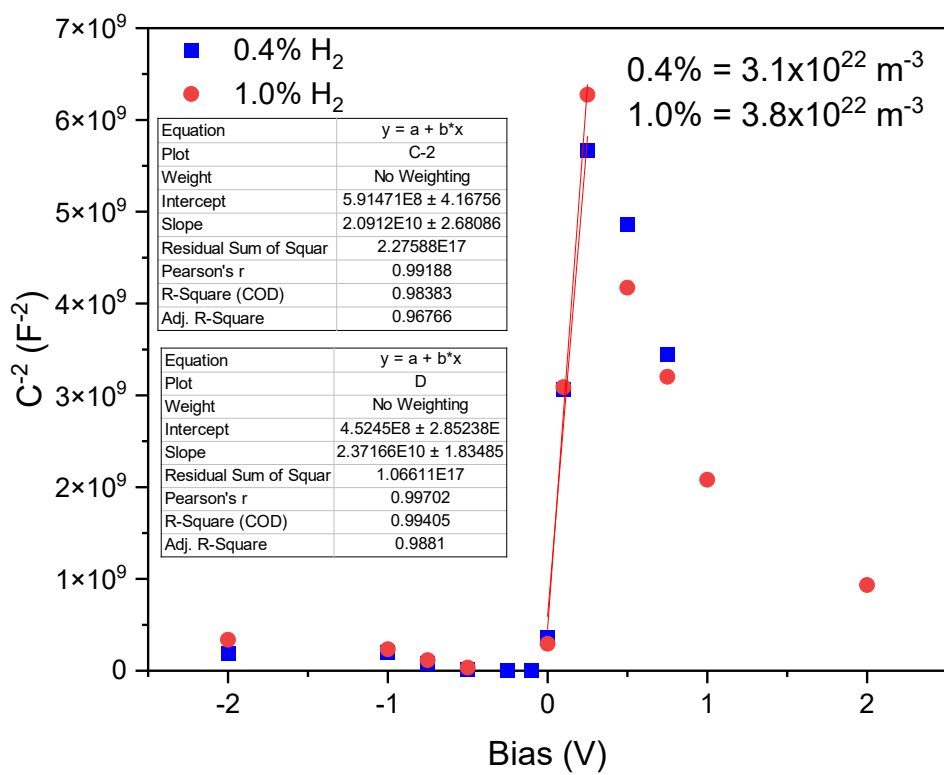


Figure S 34. Mott-Schottky plot for the BaTiO₃-Pt interface region at 22 °C under 0.4% and 1.0% H₂.

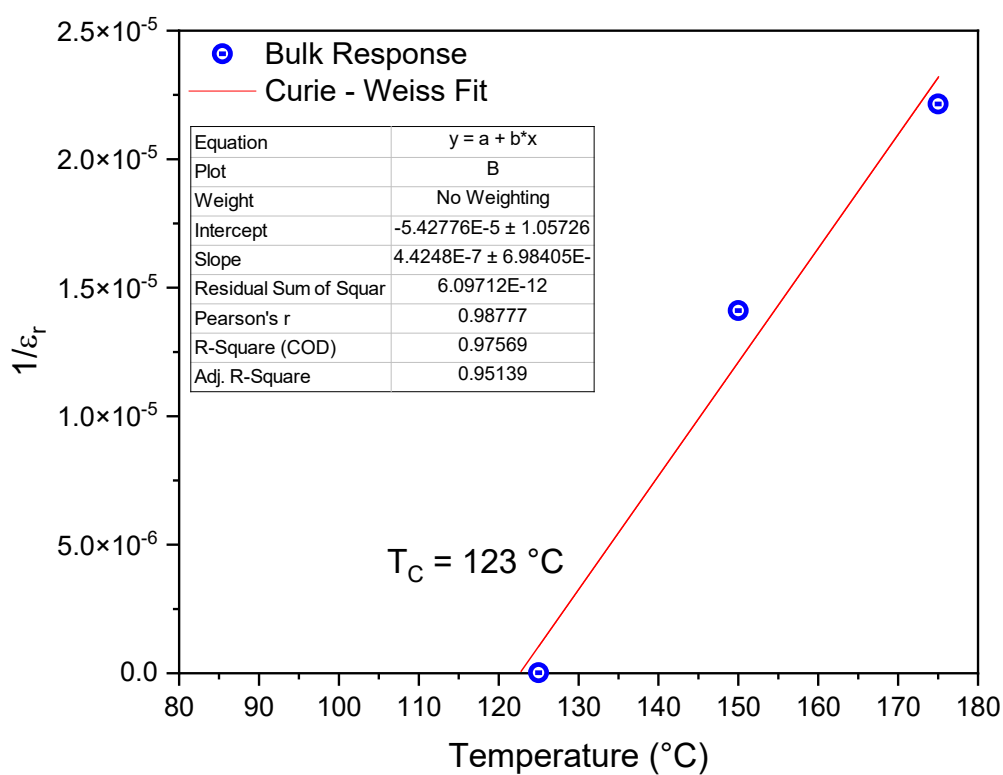
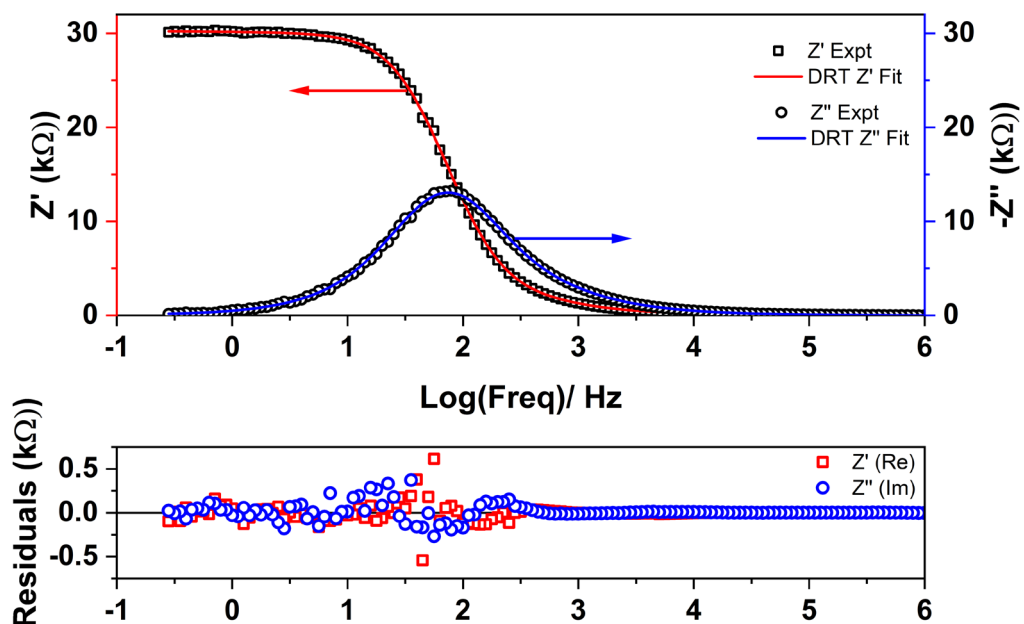


Figure S 35. Curie-Weiss plot for bulk BTO-470 under N₂. Calculated form the capacitance derived from the DRT fitting.

2.8.6 Distribution of Relaxation Times Analysis (DRT)

a)



b)

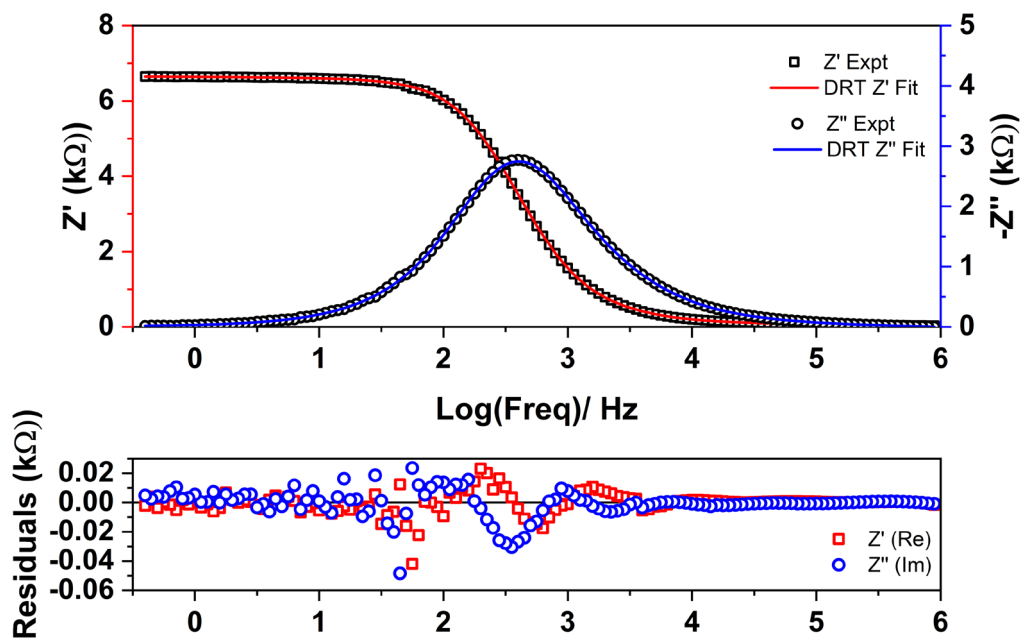


Figure S 36. Spectroscopic plots of experimental Z' and Z'' vs. frequency data and the fitting of the DRT model, with the corresponding residual data, for Pt-BTO-470 at 22 °C and under (a) pure N_2 and (b) 0.4% H_2 in N_2 .

Gauss Deconvolution of DRT Spectra to Quantify the Resistance Contribution of Each Electroactive Component

Table S 17. Gauss deconvolution of the DRT spectra for pure N₂ (0 % H₂)

Peak 1 (P1) – Electrode

Temperature	X _c of P1	w	Area	Area*2.303	Sigma	FWHM	Height	Total R ² Adjust for P1, P2, and P3	Total R for P1 + P2 + P3
(°C)	Log ₁₀ (T)/ s								
22	-1.508	0.126	57.519	132.466	0.063	0.148	364.233	0.9940	30481.8
80	-2.292	0.195	30.668	70.628	0.097	0.229	125.773	0.9938	10347.7
100	-2.446	0.116	41.064	94.570	0.058	0.136	282.883	0.9935	7417.4
125	-2.443	0.154	25.168	57.962	0.077	0.182	130.126	0.9938	5893.9
150	-2.526	0.301	54.911	126.461	0.150	0.354	145.569	0.9978	4002.8
175	-2.738	0.383	49.955	115.047	0.192	0.451	103.960	0.9996	3249.4

Peak 2(P2) – Grain Boundary

Temperature	X _c of P2	w	Area	Area*2.303	Sigma	FWHM	Height
(°C)	Log ₁₀ (T)/ s						
22	-2.664	0.422	12594.034	29004.060	0.211	0.497	23799.809
80	-3.431	0.424	4210.324	9696.375	0.212	0.500	7915.324
100	-3.597	0.410	3018.840	6952.388	0.205	0.482	5878.376
125	-3.512	0.409	2396.594	5519.356	0.204	0.481	4678.908
150	-3.584	0.476	1575.153	3627.577	0.238	0.561	2638.068
175	-3.811	0.519	1257.173	2895.269	0.259	0.611	1933.115

Peak 3 (P3) - Bulk

Temperature	X _c of P3	w	Area	Area*2.303	Sigma	FWHM	Height
(°C)	Log ₁₀ (T)/ s						
22	-3.747	0.269	584.153	1345.305	0.135	0.317	1730.596
80	-4.483	0.285	252.132	580.661	0.142	0.335	706.650
100	-4.655	0.243	160.845	370.425	0.122	0.287	527.388
125	-4.574	0.260	137.479	316.615	0.130	0.306	422.520
150	-4.613	0.324	108.023	248.777	0.162	0.381	266.422
175	-4.807	0.382	103.820	239.098	0.191	0.450	216.705

Table S 18. Gauss deconvolution of DRT spectra for 0.4% H₂ in N₂

Peak 1 (P1) – Electrode

Temperature	X _c of P1	w	Area	Area*2.303	Sigma	FWHM	Height	Total R2 Adjust for P1, P2, and P3	Total R for P1 + P2 + P3
(°C)	Log ₁₀ (T)/ s								
22	-2.322	0.158	39.354	90.633	0.079	0.185	199.370	0.9952	6574.7
80	-3.200	0.332	24.569	56.582	0.166	0.391	59.025	0.9993	1369.1
100	-3.576	0.750	24.135	55.583	0.375	0.883	25.676	0.9998	624.9
125	-3.645	0.626	9.947	22.908	0.313	0.737	12.676	0.9999	329.6
150	-4.053	0.697	9.208	21.207	0.348	0.820	10.547	0.9999	200.9
175	-4.266	0.730	3.029	6.976	0.365	0.859	3.313	0.9992	75.2

Peak 2 (P2) – Grain Boundary

Temperature	X _c of P2	w	Area	Area*2.303	Sigma	FWHM	Height
(°C)	Log ₁₀ (T)/ s						
22	-3.386	0.462	2636.068	6070.864	0.231	0.544	4554.253
80	-4.255	0.530	528.127	1216.276	0.265	0.624	795.654
100	-4.539	0.649	215.731	496.829	0.324	0.764	265.273
125	-4.650	0.696	119.606	275.453	0.348	0.819	137.191
150	-4.882	0.703	66.040	152.090	0.351	0.828	74.968
175	-5.087	0.610	18.212	41.942	0.305	0.719	23.806

Peak 3 (P3) - Bulk

Temperature	X _c of P3	w	Area	Area*2.303	Sigma	FWHM	Height
(°C)	Log ₁₀ (T)/ s						
22	-4.329	0.380	179.433	413.235	0.190	0.447	376.905
80	-5.069	0.383	41.802	96.271	0.191	0.451	87.117
100	-5.105	0.509	31.473	72.483	0.254	0.599	49.377
125	-5.558	0.500	13.560	31.228	0.250	0.588	21.659
150	-5.702	0.461	12.004	27.644	0.230	0.543	20.777
175	-5.757	0.550	11.408	26.272	0.275	0.647	16.560

Table S 19. Gauss deconvolution of DRT spectra for 1.04% H₂ in N₂

Peak 1 (P1) – Electrode

Temperature	X _c of P1	w	Area	Area*2.303	Sigma	FWHM	Height	Total R2 Adjust for P1, P2, and P3	Total R for P1 + P2 + P3
(°C)	Log ₁₀ (T)/ s								
22	22	-2.354	0.250	31.660	72.912	0.125	0.294	0.9965	5071.7
80	80	-3.272	0.337	21.043	48.461	0.168	0.396	0.9974	1266.2
100	100	-3.738	0.750	16.359	37.674	0.375	0.883	0.9997	444.6
125	125	-3.756	0.780	10.882	25.062	0.390	0.918	0.9994	272.0
150	150	-4.224	0.780	6.466	14.892	0.390	0.918	0.9998	117.2
175	175	-4.342	0.774	2.297	5.289	0.387	0.911	0.9998	63.8

Peak 2 (P2) – Grain Boundary

Temperature	X _c of P2	w	Area	Area*2.303	Sigma	FWHM	Height
(°C)	Log ₁₀ (T)/ s						
22	-3.515	0.480	2022.362	4657.500	0.240	0.566	3359.085
80	-4.315	0.517	489.523	1127.372	0.258	0.609	755.545
100	-4.722	0.710	169.393	390.113	0.355	0.836	190.430
125	-4.744	0.705	96.172	221.483	0.352	0.830	108.915
150	-5.014	0.658	32.774	75.479	0.329	0.775	39.738
175	-5.083	0.565	13.039	30.029	0.282	0.665	18.430

Peak 3 (P3) - Bulk

Temperature	X _c of P3	w	Area	Area*2.303	Sigma	FWHM	Height
(°C)	Log ₁₀ (T)/ s						
22	-4.422	0.481	148.183	341.266	0.241	0.567	245.580
80	-5.077	0.421	39.245	90.382	0.211	0.496	74.318
100	-5.129	0.390	7.305	16.824	0.195	0.459	14.947
125	-5.632	0.465	11.052	25.452	0.232	0.547	18.980
150	-5.734	0.499	11.630	26.784	0.250	0.588	18.591
175	-5.732	0.615	12.369	28.485	0.308	0.724	16.039

Table S 20. Gauss deconvolution of DRT spectra for 2.86% H₂ in N₂

Peak 1 (P1) – Electrode

Temperature	X _c of P1	w	Area	Area*2.303	Sigma	FWHM	Height	Total R2 Adjust for P1, P2, and P3	Total R for P1 + P2 + P3
(°C)	Log ₁₀ (T)/ s								
22	-2.658	0.260	61.398	141.401	0.130	0.306	188.244	0.9976	4657.1
80	-3.319	0.307	18.469	42.533	0.154	0.362	47.993	0.9969	1133.7
100	-3.803	0.650	13.710	31.573	0.325	0.765	16.829	0.9977	389.5
125	-3.834	0.780	7.554	17.398	0.390	0.918	7.728	0.9995	214.1
150	-4.430	0.928	6.548	15.080	0.464	1.093	5.629	0.9998	96.3
175	-4.191	0.534	0.934	2.152	0.267	0.629	1.396	0.9998	51.5

Peak 2 (P2) – Grain Boundary

Temperature	X _c of P2	w	Area	Area*2.303	Sigma	FWHM	Height
(°C)	Log ₁₀ (T)/ s						
22	-3.726	0.513	1818.954	4189.051	0.257	0.604	2826.924
80	-4.372	0.511	437.658	1007.925	0.256	0.602	682.965
100	-4.776	0.657	141.665	326.254	0.328	0.773	172.110
125	-4.834	0.792	74.860	172.402	0.396	0.933	75.369
150	-5.060	0.621	23.137	53.284	0.311	0.732	29.706
175	-5.115	0.592	11.170	25.724	0.296	0.697	15.051

Peak 3 (P3) - Bulk

Temperature	X _c of P3	w	Area	Area*2.303	Sigma	FWHM	Height
(°C)	Log ₁₀ (T)/ s						
22	-4.667	0.379	141.846	326.672	0.190	0.446	298.598
80	-5.051	0.410	36.129	83.206	0.205	0.483	70.310
100	-5.122	0.390	13.738	31.638	0.195	0.459	28.118
125	-5.730	0.435	10.535	24.262	0.218	0.512	19.323
150	-5.738	0.541	12.145	27.970	0.270	0.636	17.926
175	-5.775	0.569	10.236	23.574	0.284	0.670	14.355

Table S 21. Gauss deconvolution of DRT spectra for 4.63% H₂ in N₂

Peak 1 (P1) – Electrode

Temperature	X _c of P1	w	Area	Area*2.303	Sigma	FWHM	Height	Total R2 Adjust for P1, P2, and P3	Total R for P1 + P2 + P3
(°C)	Log ₁₀ (T)/ s								
22	22	-2.707	0.308	51.012	117.481	0.154	0.362	0.9982	4394.0
80	80	-3.344	0.292	18.547	42.713	0.146	0.343	0.9966	1081.6
100	100	-3.883	0.650	13.430	30.930	0.325	0.765	0.9992	345.2
125	125	-3.917	0.780	5.335	12.287	0.390	0.918	0.9996	166.2
150	150	-4.504	0.962	6.119	14.093	0.481	1.133	0.9998	87.5
175	175	-4.159	0.461	0.641	1.477	0.231	0.543	0.9999	44.7

Peak 2 (P2) – Grain Boundary

Temperature	X _c of P2	w	Area	Area*2.303	Sigma	FWHM	Height
(°C)	Log ₁₀ (T)/ s						
22	-3.773	0.505	1723.709	3969.702	0.252	0.594	2725.665
80	-4.399	0.510	418.123	962.936	0.255	0.601	653.663
100	-4.793	0.638	118.953	273.948	0.319	0.752	148.666
125	-4.899	0.813	57.179	131.684	0.407	0.958	56.093
150	-5.077	0.602	19.724	45.424	0.301	0.709	26.151
175	-5.114	0.568	8.713	20.065	0.284	0.668	12.248

Peak 3 (P3) - Bulk

Temperature	X _c of P3	w	Area	Area*2.303	Sigma	FWHM	Height
(°C)	Log ₁₀ (T)/ s						
22	-4.695	0.367	133.236	306.843	0.184	0.433	289.328
80	-5.055	0.390	32.996	75.989	0.195	0.459	67.504
100	-5.127	0.388	17.489	40.277	0.194	0.456	35.993
125	-5.748	0.453	9.664	22.257	0.227	0.534	17.014
150	-5.740	0.548	12.164	28.014	0.274	0.645	17.721
175	-5.776	0.579	10.075	23.204	0.290	0.682	13.878

Table S 22. Gauss deconvolution of DRT spectra for 6.33% H₂ in N₂

Peak 1 (P1) – Electrode

Temperature	X _c of P1	w	Area	Area*2.303	Sigma	FWHM	Height	Total R2 Adjust for P1,P2, and P3	Total R for P1 + P2 + P3
(°C)	Log ₁₀ (T)/ s								
22	-2.736	0.271	50.303	115.847	0.135	0.319	148.305	0.9971	4301.7
80	-3.331	0.312	17.621	40.581	0.156	0.367	45.070	0.9966	1055.0
100	-3.900	0.650	12.089	27.842	0.325	0.765	14.840	0.9988	321.5
125	-4.073	0.780	6.067	13.972	0.390	0.918	6.206	0.9996	149.9
150	-4.214	0.615	2.669	6.147	0.308	0.724	3.462	0.9996	84.3
175	-4.154	0.462	0.592	1.363	0.231	0.544	1.022	0.9997	41.7

Peak 2 (P2) – Grain Boundary

Temperature	X _c of P2	w	Area	Area*2.303	Sigma	FWHM	Height
(°C)	Log ₁₀ (T)/ s						
22	-3.793	0.503	1687.865	3887.153	0.251	0.592	2678.244
80	-4.416	0.519	409.996	944.221	0.260	0.612	629.737
100	-4.820	0.655	113.348	261.040	0.328	0.772	137.979
125	-4.934	0.756	48.065	110.695	0.378	0.890	50.748
150	-5.069	0.648	23.588	54.324	0.324	0.762	29.063
175	-5.112	0.547	7.535	17.352	0.273	0.644	10.997

Peak 3 (P3) - Bulk

Temperature	X _c of P3	w	Area	Area*2.303	Sigma	FWHM	Height
(°C)	Log ₁₀ (T)/ s						
22	-4.709	0.371	129.707	298.715	0.185	0.437	279.134
80	-5.063	0.410	30.460	70.150	0.205	0.483	59.277
100	-5.117	0.369	14.183	32.663	0.185	0.435	30.635
125	-5.740	0.484	10.960	25.242	0.242	0.569	18.083
150	-5.751	0.504	10.326	23.781	0.252	0.593	16.352
175	-5.776	0.593	9.985	22.995	0.297	0.699	13.428

Table S 23. Gauss deconvolution of DRT spectra for 7.97% H₂ in N₂

Peak 1 (P1) – Electrode

Temperature	X _c of P1	w	Area	Area*2.303	Sigma	FWHM	Height	Total R2 Adjust for P1,P2, and P3	Total R for P1 + P2 + P3
(°C)	Log ₁₀ (T)/ s								
22	-2.749	0.274	45.418	104.597	0.137	0.322	132.338	0.9970	4265.8
80	-3.413	0.267	14.126	32.533	0.134	0.315	42.146	0.9965	1012.6
100	-3.930	0.650	11.787	27.146	0.325	0.765	14.469	0.9995	307.3
125	-4.089	0.780	5.563	12.812	0.390	0.918	5.691	0.9997	139.2
150	-4.386	0.838	3.869	8.909	0.419	0.987	3.682	0.9998	81.2
175	-4.158	0.445	0.532	1.226	0.222	0.523	0.955	0.9998	41.1

Peak 2 (P2) – Grain Boundary

Temperature	X _c of P2	w	Area	Area*2.303	Sigma	FWHM	Height
(°C)	Log ₁₀ (T)/ s						
22	-3.801	0.496	1675.951	3859.714	0.248	0.584	2697.275
80	-4.495	0.497	397.584	915.636	0.248	0.585	638.753
100	-4.817	0.640	102.101	235.139	0.320	0.753	127.379
125	-4.959	0.750	44.324	102.078	0.375	0.883	47.140
150	-5.074	0.590	19.058	43.891	0.295	0.695	25.753
175	-5.106	0.534	6.844	15.763	0.267	0.629	10.219

Peak 3 (P3) - Bulk

Temperature	X _c of P3	w	Area	Area*2.303	Sigma	FWHM	Height
(°C)	Log ₁₀ (T)/ s						
22	-4.709	0.379	130.924	301.517	0.190	0.447	275.369
80	-5.050	0.420	27.990	64.462	0.210	0.495	53.174
100	-5.121	0.412	19.525	44.967	0.206	0.485	37.841
125	-5.753	0.477	10.551	24.298	0.238	0.562	17.652
150	-5.739	0.555	12.349	28.440	0.278	0.654	17.744
175	-5.775	0.620	10.484	24.144	0.310	0.730	13.483

Table S 24. Deconvolution of DRT spectra for 19.16% H₂ in N₂

Peak 1 (P1) – Electrode

Temperature	X _c of P1	w	Area	Area*2.303	Sigma	FWHM	Height	Total R2 Adjust for P1,P2, and P3	Total R for P1 + P2 + P3
(°C)	Log ₁₀ (T)/ s								
22	-2.738	0.260	46.518	107.131	0.130	0.307	142.559	0.9965	4190.3
80	-3.400	0.282	13.765	31.700	0.141	0.331	39.011	0.9966	972.0
100	-3.977	0.650	12.136	27.950	0.325	0.765	14.897	0.9992	292.1
125	-4.126	0.780	5.399	12.434	0.390	0.918	5.523	0.9997	130.7
150	-4.381	0.888	3.669	8.450	0.444	1.046	3.297	0.9995	78.9
175	-4.152	0.414	0.477	1.097	0.207	0.488	0.918	0.9999	38.5

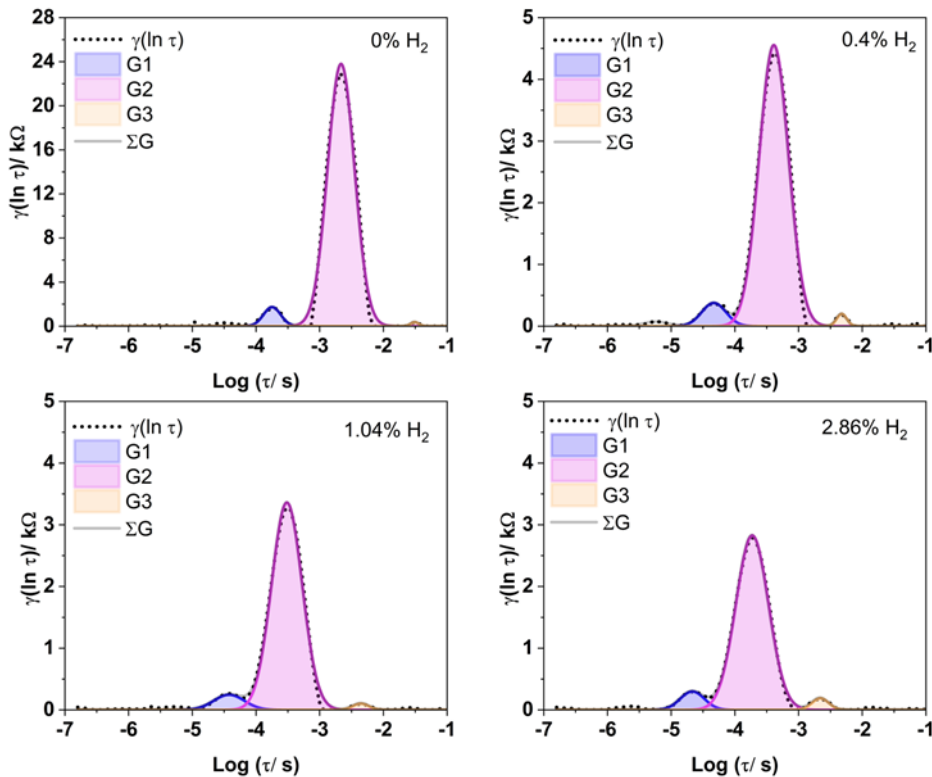
Peak 2 (P2) – Grain Boundary

Temperature	X _c of P2	w	Area	Area*2.303	Sigma	FWHM	Height
(°C)	Log ₁₀ (T)/ s						
22	-3.824	0.490	1648.460	3796.404	0.245	0.576	2686.363
80	-4.524	0.508	387.353	892.073	0.254	0.599	607.945
100	-4.831	0.610	94.040	216.573	0.305	0.718	122.982
125	-4.986	0.722	40.565	93.420	0.361	0.851	44.802
150	-5.072	0.583	17.991	41.434	0.291	0.686	24.636
175	-5.127	0.538	6.607	15.216	0.269	0.633	9.800

Peak 3 (P3) - Bulk

Temperature	X _c of P3	w	Area	Area*2.303	Sigma	FWHM	Height
(°C)	Log ₁₀ (T)/ s						
22	-4.730	0.364	124.531	286.795	0.182	0.428	273.251
80	-5.070	0.410	20.938	48.220	0.205	0.483	40.746
100	-5.124	0.402	20.664	47.589	0.201	0.473	41.045
125	-5.754	0.486	10.799	24.871	0.243	0.572	17.727
150	-5.721	0.561	12.580	28.972	0.280	0.660	17.895
175	-5.789	0.589	9.627	22.172	0.294	0.693	13.048

a)



b)

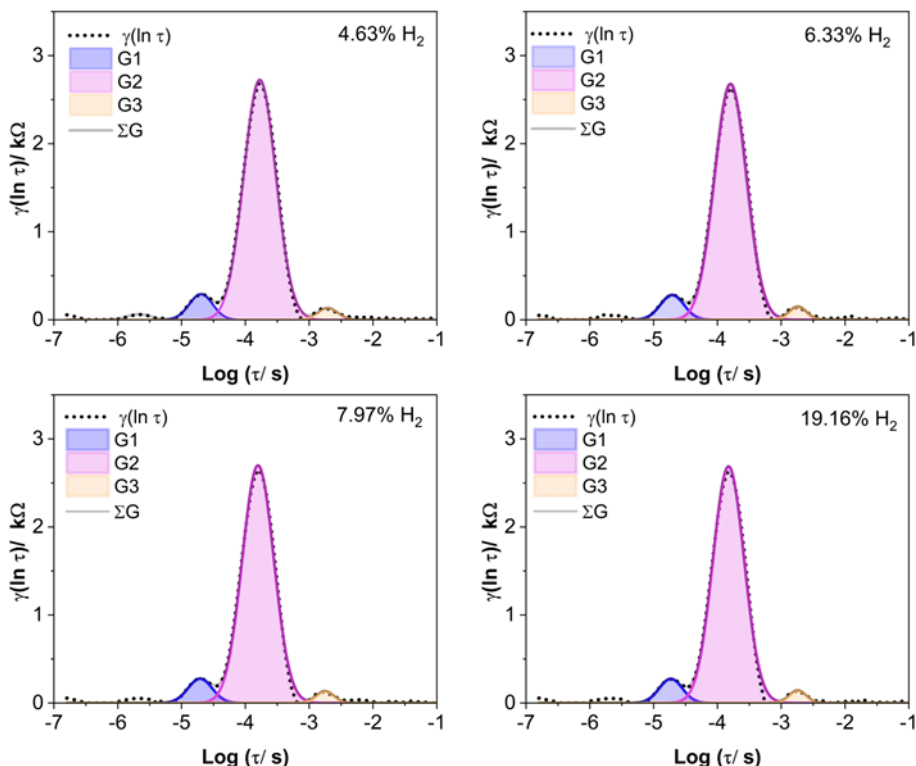
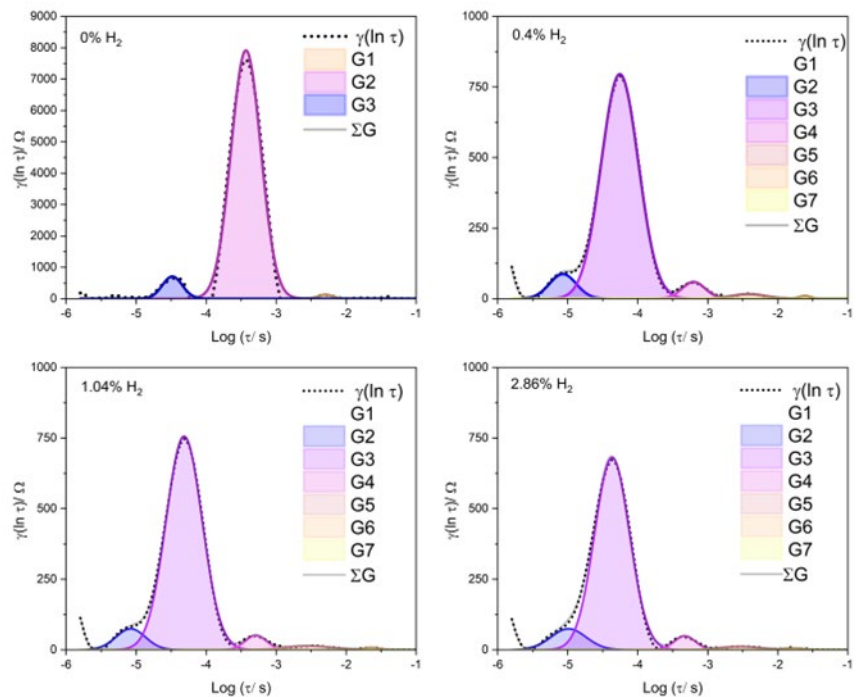


Figure S 37. Gauss deconvolution of DRT spectra for impedance measurements at 22 °C for gall $\text{H}_2 + \text{N}_2$ mixtures studied.

a)



b)

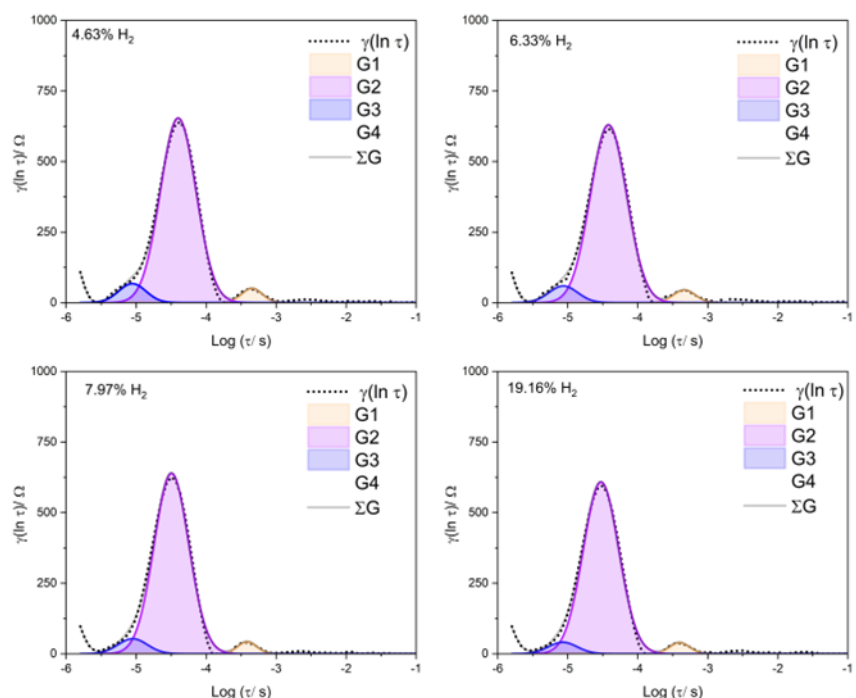
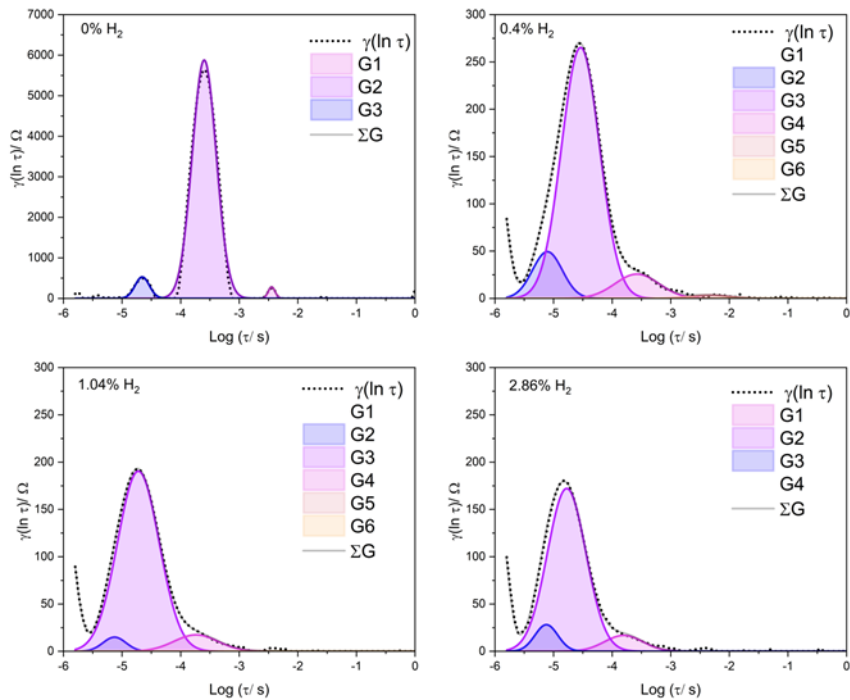


Figure S 38. Gauss deconvolution of DRT spectra for impedance measurements at 80 °C for all $H_2 + N_2$ mixtures studied.

a)



b)

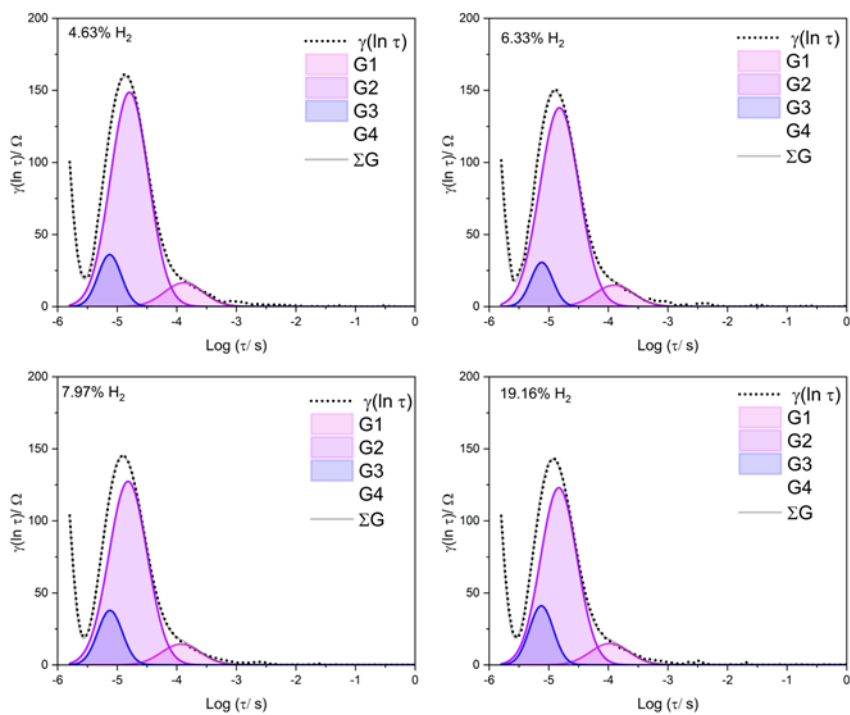
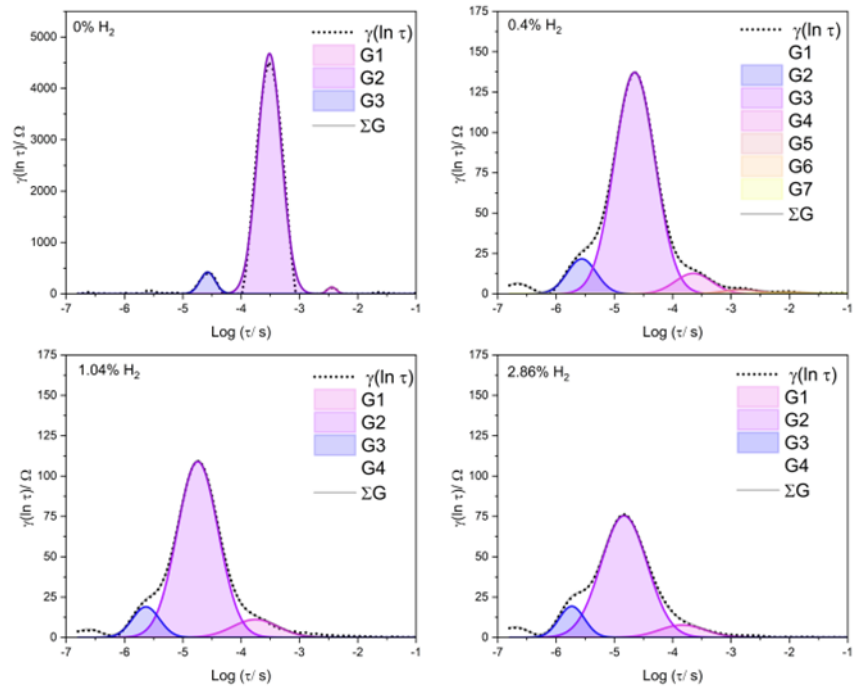


Figure S 39. Gauss deconvolution of DRT spectra for impedance measurements at 100 °C for all $\text{H}_2 + \text{N}_2$ mixtures studied.

a)



b)

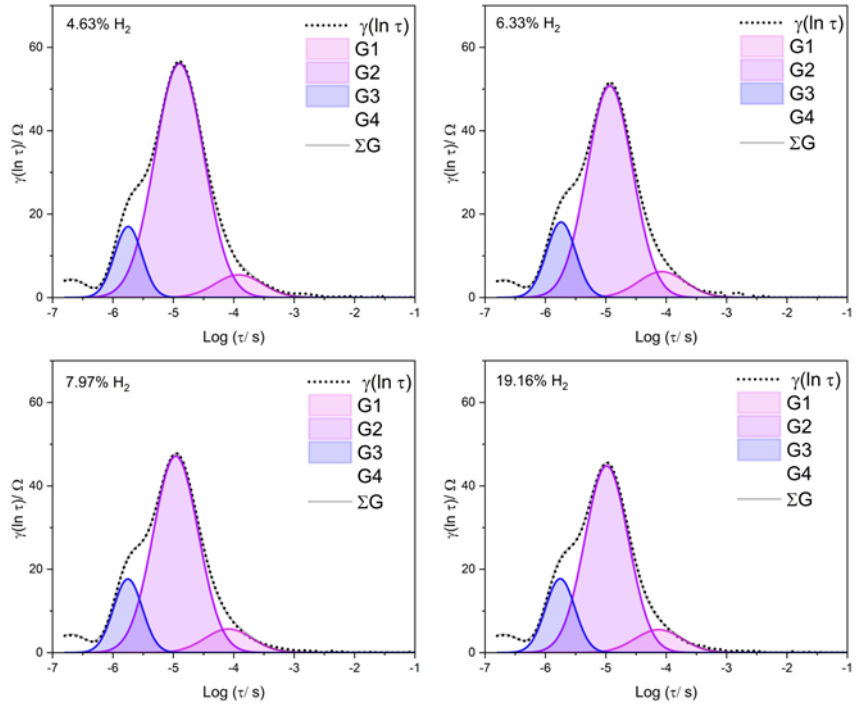
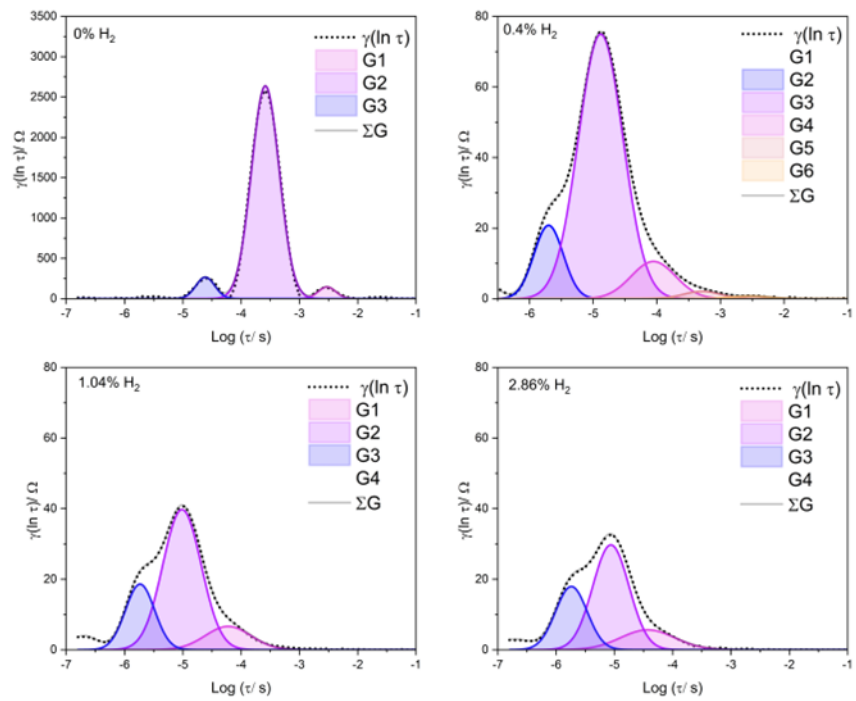


Figure S 40. Gauss deconvolution of DRT spectra for impedance measurements at 125 °C for all $\text{H}_2 + \text{N}_2$ mixtures studied.

a)



b)

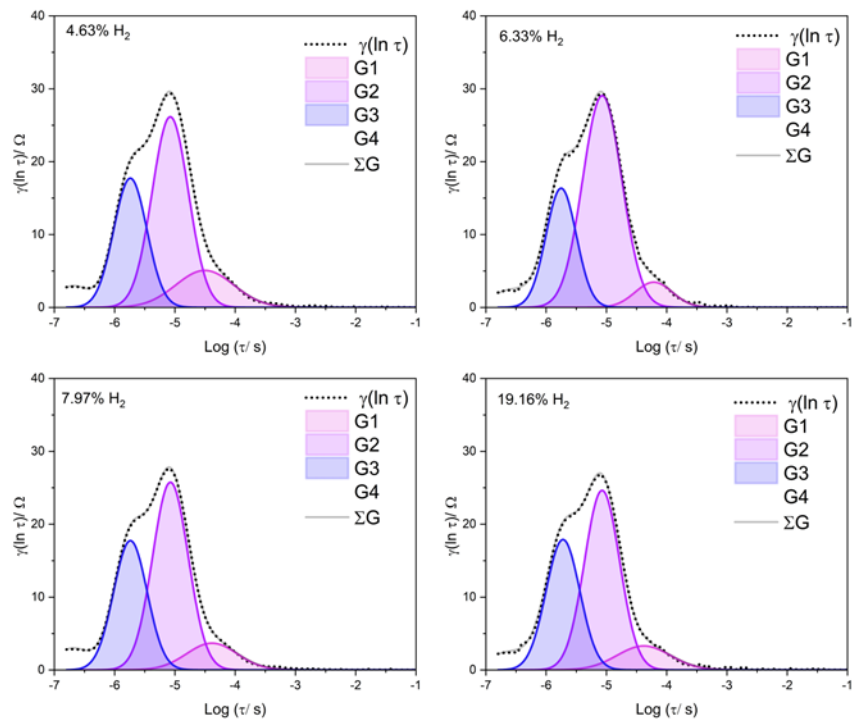
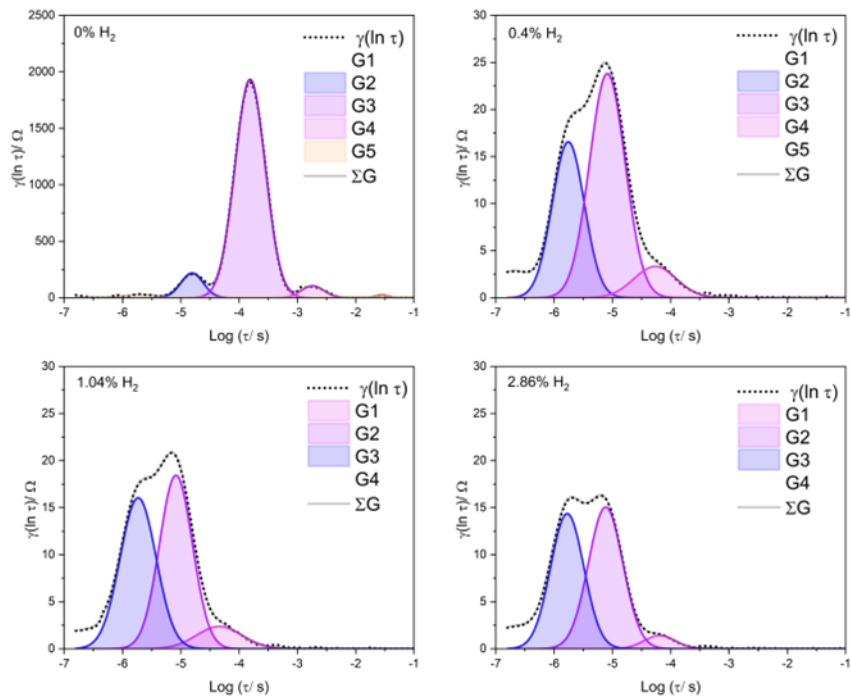


Figure S 41. Gauss deconvolution of DRT spectra for impedance measurements at 150 °C for all $\text{H}_2 + \text{N}_2$ mixtures studied.

a)



b)

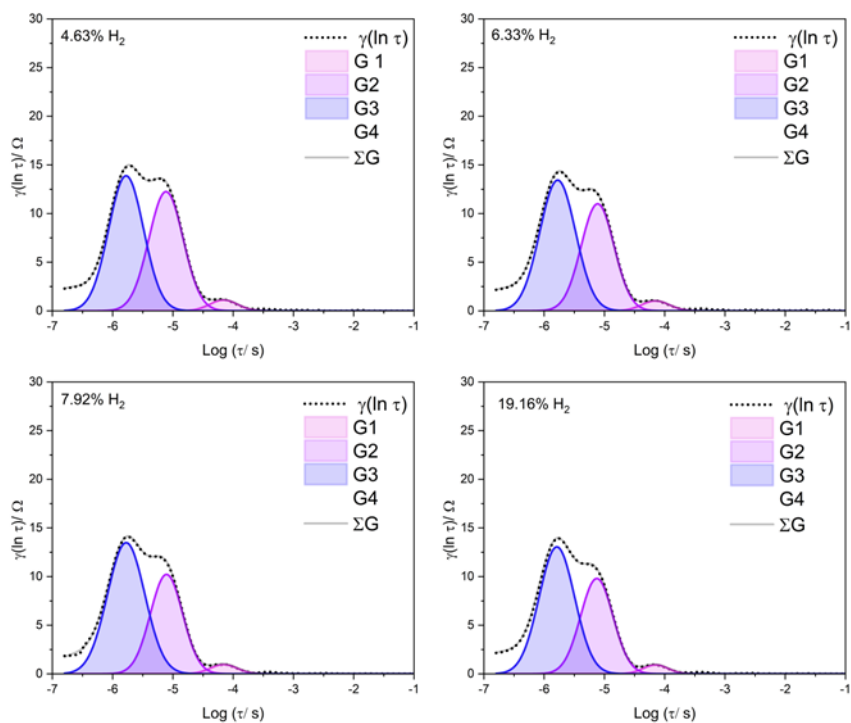


Figure S 42. Gauss deconvolution of DRT spectra for impedance measurements at 175 °C for all H₂ + N₂ mixtures studied.

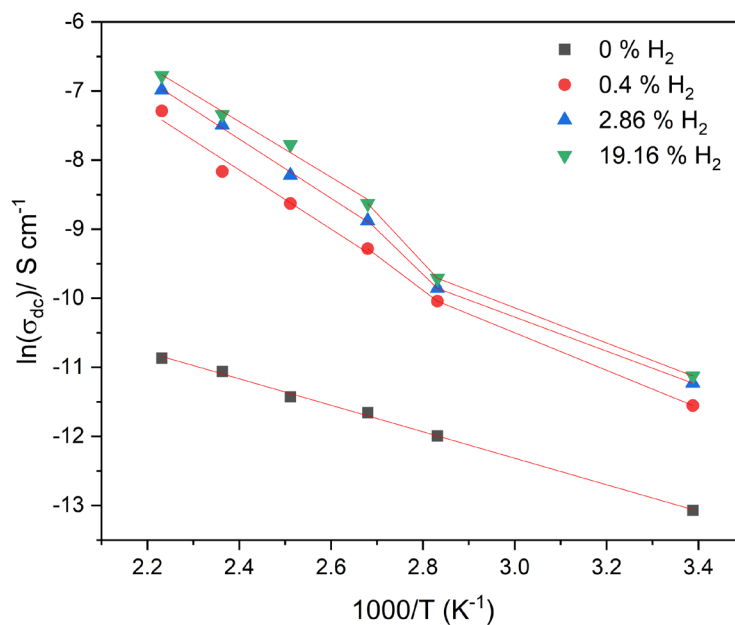
2.8.7 Activation Energies from Jonscher Analysis using σ_{dc} Data

Table S 25. Activation energies for Pt-BTO-470 as a function of H₂ concentration. Values derived from three temperature-dependent linear regions of DC conductivity vs. 1/ T obtained from Jonscher analysis of impedance spectra.

H ₂ Concentration (%)	Activation Energy (eV)		
	T ^a < 80 °C	80 °C < T ^b < 100 °C	T ^c > 100 °C
0	0.17		
0.4	0.23	0.43	0.37 ± 0.10
1.04	0.21	0.57	0.36 ± 0.06
2.86	0.21	0.56	0.37 ± 0.03
4.63	0.21	0.59	0.36 ± 0.03
6.33	0.21	0.61	0.36 ± 0.04
7.91	0.22	0.61	0.35 ± 0.05
19.16	0.22	0.62	0.35 ± 0.06

a = 2 points, b = 2 points, c = 4 points used in the Arrhenius plot

a)



b)

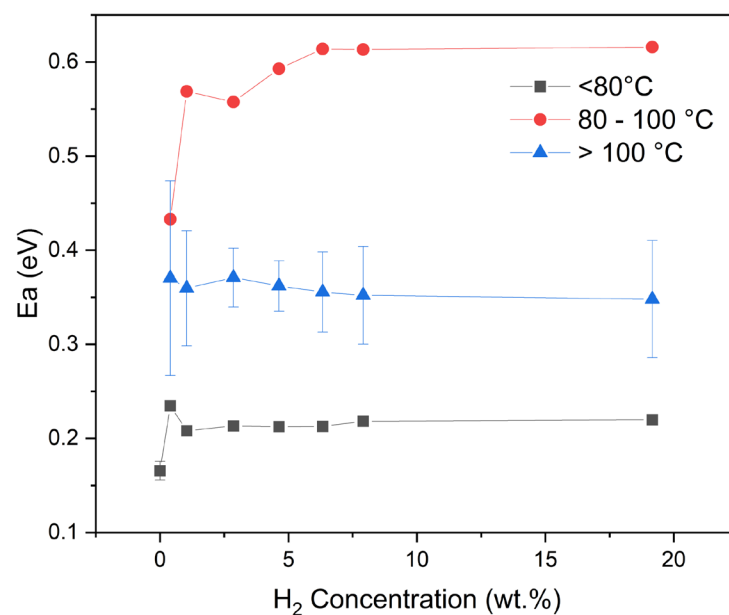


Figure S 43. (a) Arrhenius plot of DC conductivities (σ_{dc}) derived from the Jonscher model vs. $1/T$ for mixtures of $H_2 + N_2$ at 0%, 0.4%, 2.9%, and 19% H_2 , and showing three temperature dependent linear regions. (b) Activation energies for electron transport derived from three linear regions in the Arrhenius plots corresponding to $T < 80^\circ\text{C}$, $T = 80 - 100^\circ\text{C}$, and $T > 100^\circ\text{C}$.

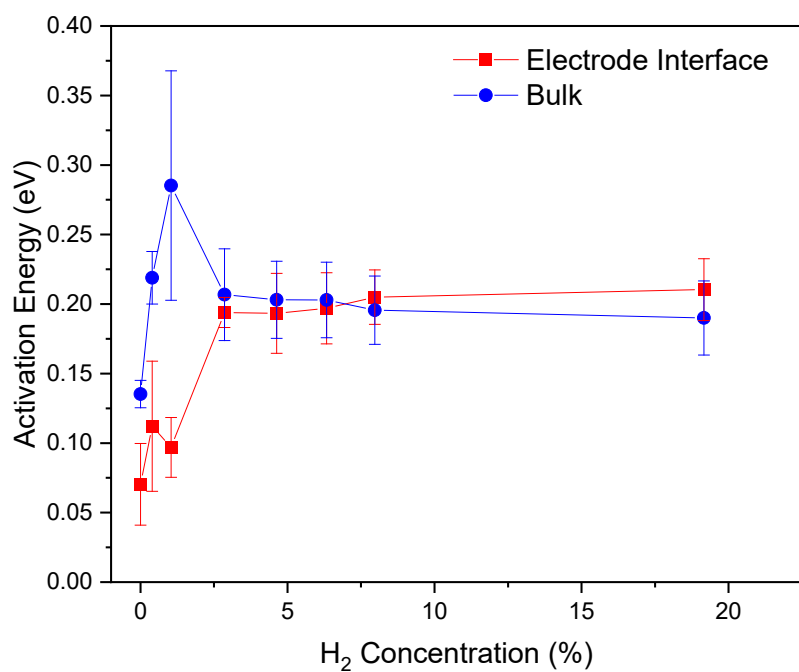
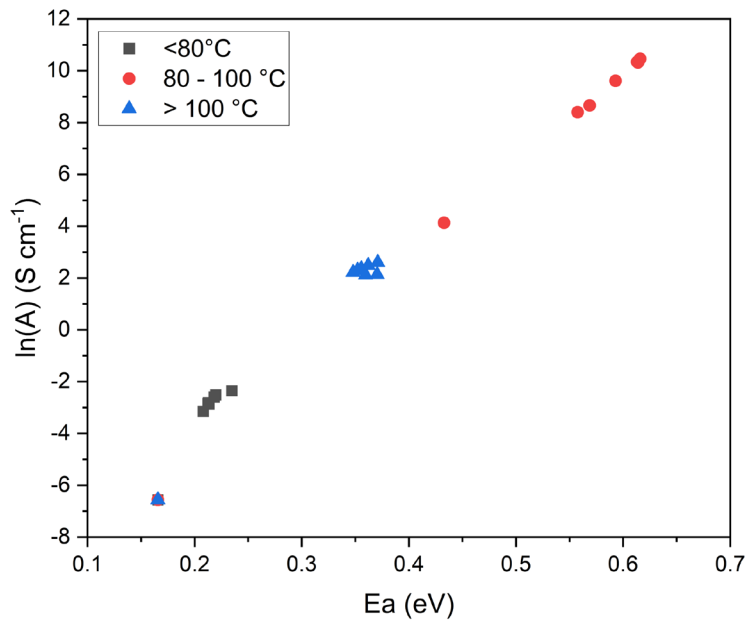


Figure S 44. Activation energy (eV) vs. H_2 concentration (%) for bulk and electrode interface regions.

2.8.8 Meyer-Neldel Effect for Total Conductivity from Jonscher σ_{dc} Data

a)



b)

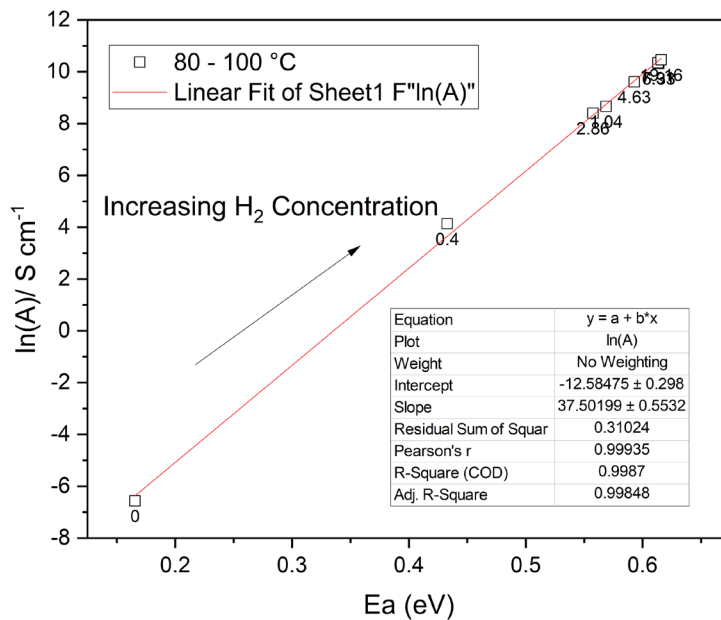


Figure S 45. (a) $\ln(A)$ vs. E_a plots for the three linear regions identified in the Arrhenius plots $T < 80^\circ\text{C}$ (black), $T = 80 - 100^\circ\text{C}$ (red), and $T > 100^\circ\text{C}$ (blue). (b) $\ln(A)$ vs. $\ln(E_a)$ plots for the temperature region $80 - 100^\circ\text{C}$ showing a progressive linear increase in $\ln(A)$ and E_a with increasing H_2 concentration (with H_2 concentrations next to symbols).

2.8.9 Grain Boundary Activation Energies from DRT Analysis

Table S 26. Activation energies for Pt-BTO-470 as a function of H₂ concentration for the Pt-BTO-470 grain boundary region. Values derived from three temperature-dependent linear regions of R_{gb} vs. 1/T obtained from Gauss deconvolution of DRT analysis of impedance spectra.

H ₂ Concentration (%)	Activation Energy (eV)		
	T ^a < 80 °C	80 °C < T ^b < 100 °C	T ^c > 100 °C
0	0.17		
0.4	0.25	0.51	0.46 ± 0.09
1.04	0.22	0.60	0.50 ± 0.06
2.86	0.22	0.64	0.51 ± 0.05
4.63	0.22	0.72	0.51 ± 0.04
6.33	0.22	0.73	0.51 ± 0.05
7.91	0.22	0.77	0.52 ± 0.04
19.16	0.23	0.81	0.51 ± 0.04

a = 2 points, b = 2 points, c = 4 points used in the Arrhenius plot

2.8.10 Meyer-Neldel Effect for Grain Boundary Regions from Distribution of Relaxation Times Analysis

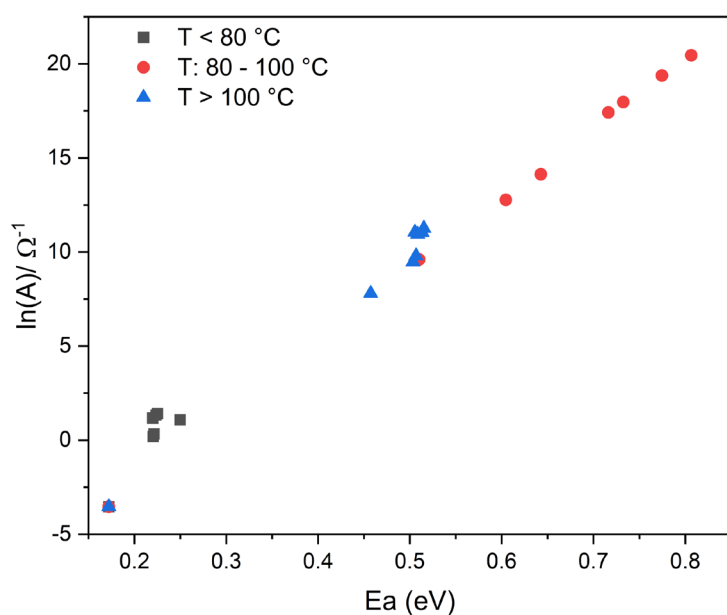


Figure S 46. Plot showing the correlation between ln(A) vs. Ea for the grain boundary region for the temperature ranges T < 80 °C, T = 80 – 100 °C, and T > 100 °C, and the progressive linear increase as the H₂ concentration is increased.

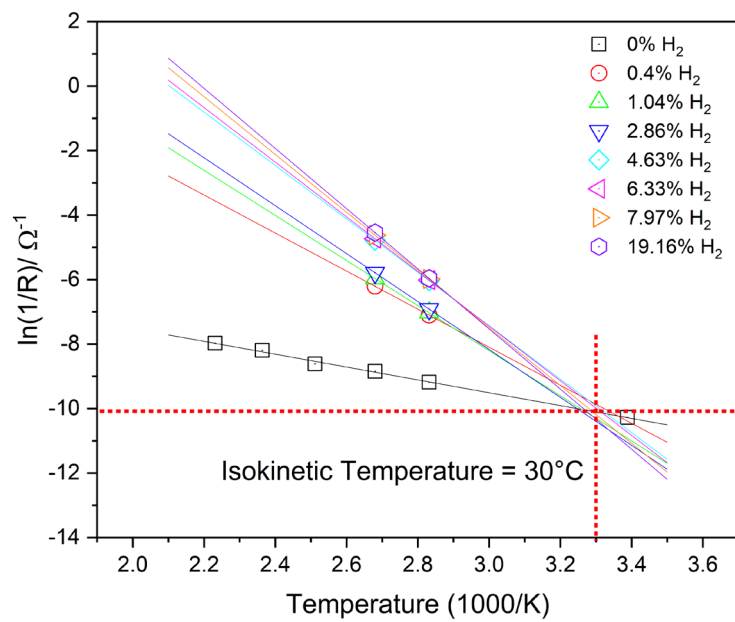


Figure S 47. Arrhenius plots of $\ln(1/R_{gb})$ vs. $1000/T$ for the Pt-BTO-470 grain boundary region and for H_2 concentrations from 0% to 19%. The appearance of an isokinetic temperature over the temperature range $T = 80 - 100^\circ\text{C}$ occurs at 30°C .

3 References

1. Singh, B.; Hesse, R.; Linford, M., Good Practices for XPS (and other Types of) Peak Fitting. Use Chi Squared, Use the Abbe Criterion, Show the Sum of Fit Components, Show the (Normalized) Residuals, Choose an Appropriate Background, Estimate Fit Parameter Uncertainties, Limit the Number of Fit Parameters, Use Information from Other Techniques, and Use Common Sense. *Vacuum Technology & Coating* **2015**.
2. Miot, C.; Husson, E.; Proust, C.; Erre, R.; Coutures, J. P., X-ray photoelectron spectroscopy characterization of barium titanate ceramics prepared by the citric route. Residual carbon study. *Journal of Materials Research* **1997**, 12 (9), 2388-2392.
3. Nishimoto, A.; Nishi, C., Carbide layer coating on titanium by spark plasma sintering technique. *Surface and Coatings Technology* **2018**, 353, 324-328.
4. Zhang, L.; Koka, R. V., A study on the oxidation and carbon diffusion of TiC in alumina–titanium carbide ceramics using XPS and Raman spectroscopy. *Mater Chem Phys* **1998**, 57 (1), 23-32.
5. Moulder, J. F.; Chastain, J., *Handbook of X-ray Photoelectron Spectroscopy: A Reference Book of Standard Spectra for Identification and Interpretation of XPS Data*. Physical Electronics Division, Perkin-Elmer Corporation: 1992.